8-31-1990

Conditional artificial dielectric waveguide

Hsien-Wen Ho
New Jersey Institute of Technology

Copyright Warning & Restrictions

The copyright law of the United States (Title 17, United States Code) governs the making of photocopies or other reproductions of copyrighted material.

Under certain conditions specified in the law, libraries and archives are authorized to furnish a photocopy or other reproduction. One of these specified conditions is that the photocopy or reproduction is not to be "used for any purpose other than private study, scholarship, or research." If a, user makes a request for, or later uses, a photocopy or reproduction for purposes in excess of "fair use" that user may be liable for copyright infringement,

This institution reserves the right to refuse to accept a copying order if, in its judgment, fulfillment of the order would involve violation of copyright law.

Please Note: The author retains the copyright while the New Jersey Institute of Technology reserves the right to distribute this thesis or dissertation

Printing note: If you do not wish to print this page, then select "Pages from: first page # to: last page #" on the print dialog screen

ABSTRACT

Title of Thesis : Conditional Artifical Dielectic Waveguide

Hsien-Wen Ho, Master of Science, 1990

Thesis directed by : Dr. Marek Sosnowski
Professor of Electrical Engineering

Dr. Haim Grebel
Professor of Electrical Engineering

A thin layer of semiconductor (the guest material) is sandwiched between two polymeric films (the host material) to form an artificial dielectric waveguide. An artificial dielectric is a composite material consisting of a dielectric with a large number of conducting particles arranged in a three-dimensional pattern. The particle dimensions are smaller than the optical wavelength of interest. A beam of light with a photon energy above the band-gap of the semiconductor (pump light) induces electric and magnetic dipoles which affect the propagation of light with a photon energy below the band-gap (probe light) in a slab waveguide.

The polymeric films have been prepared using plasma polymerization technique. The film of cadmium sulfide was embedded in the polymeric

film by vapor deposition. The film structure and average thickness of CdS were measured using Rutherford Backscattering Spectrometry and Scanning Electron Microscope.

The waist of the near-field intensity pattern of a polymer - semiconductor - polymer waveguide was changed up to 15% for a clustered semiconductor film under the illumination from a white light source. Almost no change was detected for a continuous semiconductor film.

2) CONDITIONAL ARTIFICIAL DIELECTRIC WAVEGUIDE

by

1) **Hsien-Wen Ho**

Thesis submitted to the Faculty of the Graduate School
of New Jersey Institute of Technology
in partial fulfillment of the requirements
of the degree of Master of Science
in Electrical Engineering

1990

APPROVAL SHEET

Title of Thesis : Conditional Artificial Dielectric Waveguide

Name of Candidate : Hsien-Wen Ho

Master of Science in Electrical Engineering, 1990

Thesis and Abstract Approvaed: _____ 08-28-90

Dr. Márek Sosnowski Date
Professor of E.E. Department

_____ Aug. 28, 90

Dr. Haim Grebel Date
Professor of E.E. department

_____ 8/28/90

Dr. Eugene Gordon Date
Professor of E E. Department

VITA

Name : Hsien-Wen Ho

Permanent address :

Degree and date to be conferred : M.S.E.E., 1990

Date of birth :

Place of birth :

Secondary education : Hwa-Shiah Junior College

Collegiate institutions attended	Degree	Date of degree
Tamgkang University	B.S.Appl.Physics	May 1988
NJIT	M.S.E.E.	Oct 1990

ACKNOWLEDGMENTS

I would like to take this opportunity to thank a number of people who assisted me during this work. I am indebted to Dr. Marek Sosnowski, Dr. Haim Grebel, Dr. Eugene Gordon for their guidance and assistance in this project. I would also like to thank Dr. Walter Brown and Dr Ji-Hyun Chung for their assistance to measure the CdS film structure. Sincere thanks to Pei-Chen Pien and Jeff Wang for their support and help during the experiment.

CONTENTS

List of Figures

List of Tables

CHAPTER 1 INTRODUCTION

There are a number of advantages in optical integrated circuits, such as high speed and large information capacity, low loss coupling, compared with similar electrical integrated circuits. However, those superior characteristics are mainly limited by the relatively high cost of developing this technology.

The choice of materials for an optical integrated circuit depends strongly on the function to be performed by the circuit. In most cases, the optical integrated circuit may consist of a number of different optical devices such as source, modulator and detectors, and no material will be optimum for all of them. So far inorganic materials, mainly semiconductors, have been studied thoroughly for electro-optic and optical intensity effects.

The interest in nonlinear optics and in particular in light-induced index of refraction and absorption change is due to its possible applications in optoelectronic devices.

In this thesis, we are reporting experimental results obtained on a thin layer of cadmium sulfide (CdS) embedded between two layers of polymeric (PMMA) waveguide. These three layers form an artificial

dielectric waveguide as shown in Fig.1-1

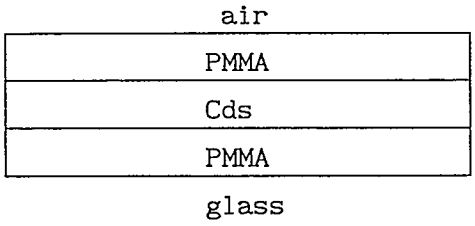

Fig 1-1 The waveguide structure

In many applications, thin film dielectric waveguides are desirable since they can be deposited conformably on various substrates, and the fabrication process is quite reliable. Several different techniques have been developed to deposit polymeric films on amorphous substrates. In the solution deposit techniques such as spinning[1] and dipping a substrate is covered with liquid photoresist[2], epoxy[3], polymethyl methacrylate[4] (PMMA), or polyurethane[3,5]. The thickness of liquid layer is controlled by either spinning the substrate at a rate of several thousand rpm in an axis perpendicular to its surface, vertically dipping the substrate into the liquid and moving it at a controlled rate, or covering the substrate with liquid and subsequently turning it upright to allow excess liquid to run off.

Another method for the deposition of polymer film is plasma polymerization. In plasma polymerization,an electrical discharge is created in a vapor containing low-weight organic molecules called monomers. The discharge causes an ionization and fragmentation of the monomers and a subsequent rebonding of the fragments into a much larger two- or three- dimensional structure by a process called

polymerization. Polymers may bond into a larger structure by cross-linking. When a substrate such as glass is introduced into the discharge in a gas containing monomer vapor, the polymer is deposited on its surface.[6]

There are some advantages of plasma polymerization in comparison with solution deposition : (1) smoother film, (2) accurate control of the thickness of the film, (3) lower optical attenuation.[3,7]

An artificial dielectric is a composite material consisting of a dielectric with a large number of conducting particles arranged in a three-dimensional pattern. The particles dimensions are smaller than the optical wavelength of interest. Under the action of an external applied electric field, the charges on each conducting particle are displaced so as to set up an induced field that will cancel the applied field at the particle surface. The particles are electrically neutral so that the dominant part of the induced field is a dipole field. Each particle thus simulates the behavior of a molecule (or a group of molecules) in an ordinary dielectric in that it exhibits a dipole moment. Light may induce changes in the dielectric properties of such a system. A beam of light with a photon energy above the band-gap of semiconductor (pump light) induces electric and magnetic dipoles which affect the propagation of a second beam of light with a photon energy below the band-gap (probe light).

In this work, we prepared an artificial dielectric composed of a

semiconductor (CdS) in a polymer (PMMA) matrix. Plasma polymerization was used to prepare polymeric films. The film of cadmium sulfide was deposited on a PMMA film by vapor deposition in a high vacuum evaporator.

The purpose of this study was to investigate the role of a pump light in changing the refractive index of the artificial dielectric. Waveguides made of such materials may become important components of new optoelectronic devices.

CHAPTER 2 ARTIFICIAL DIELECTRIC WAVEGUIDE

2.1 TE and TM Mode in an Asymmetric Waveguide

Light is confined to a dielectric waveguide because the refractive index of the guide medium is larger than its surrounding cladding layer. In our case, the air (refractive index $n_a = 1$) and a glass substrate (refractive index $n_g = 1.49$) confine the light to a composite guiding layer (refractive index $n_{wg} > 1.49$). Light propagates in the waveguide as long as the transverse boundary conditions are fulfilled. Stable solutions of the wave equation are called mode of propagation. We solve Maxwell's equations for the transverse mode assuming propagation along the waveguide in the form of $\mathbb{E}(z) = E_0 e^{i(\omega t - \beta z)}$, thus,

$$\nabla^2 \mathbb{E}(r) + k_0^2 n^2(r) \mathbb{E}(r) = 0. \qquad 2.1.1$$

Here $k_0^2 \equiv \omega^2 \mu\varepsilon_0 = (2\pi/\lambda)^2$, and n is the index of refraction in the region of interest. The solutions are subject to the continuity of the tangential components of E and H at the dielectric interface, so that Eq.(2.1.1) becomes

$$\left(\frac{\partial^2}{\partial x^2} + \frac{\partial^2}{\partial y^2} \right) \mathbb{E}(x,y) + (k_0^2 n^2(r) - \beta^2) \mathbb{E}(x,y) = 0 \qquad 2.1.2$$

Consider a slab waveguide, where $n_2 > n_3 > n_1$ lets $\partial E/\partial y = 0$. Then Eq. (2.1.2) becomes

$$\frac{\partial^2}{\partial x^2} \mathbb{E}(x,y) + (k_0^2 n_1^2 - \beta^2) \mathbb{E}(x,y) = 0 \qquad 0 \le x < \infty \qquad 2.1.3a$$

$$\frac{\partial^2}{\partial x^2} \mathbb{E}(x,y) + (k_0^2 n_2^2 - \beta^2) \mathbb{E}(x,y) = 0 \qquad -t \le x \le 0 \qquad 2.1.3b$$

$$\frac{\partial^2}{\partial x^2} \mathbb{E}(x,y) + (k_0^2 n_3^2 - \beta^2) \mathbb{E}(x,y) = 0 \qquad -\infty < x \le -t \qquad 2.1.3c$$

2.1.1 TE Mode

Two polarization eigenstates are solutions to Eqs (2.1.3); the TE and TM states. TE has no electric component in the $\hat{z}$ direction while TM has no magnetic component in the $\hat{z}$ direction. The components of the TE mode are :

$$Ey(x,z,t) = \mathbb{E}(x)\, e^{i(\omega t - \beta z)}$$

$$Hz(x,z,t) = \frac{i}{\mu\omega} \left(\frac{\partial\, \mathbb{E}y}{\partial\, x} \right) \qquad 2.1.5$$

$$Hx(x,z,t) = \frac{-i}{\mu\omega} \left(\frac{\partial\, \mathbb{E}y}{\partial\, x} \right) \qquad 2.1.6$$

the mode function $\mathbb{E}y(x)$ is taken as

$$\mathbb{E}y = \begin{cases} C\, e^{-qx}, & 0 \le x \le \infty \\ C \left[\cos(ht) - \frac{q}{h} \sin(ht), \right. & -t \le x \le 0 \\ C \left[\cos(ht) - \frac{q}{h} \sin(ht) \right] e^{p(x+t)} & -\infty < x < -t \end{cases} \qquad 2.1.7$$

Substitution of Eq. (2.1.7) into Eq (2.1.4) leads to

$$h = (n_1^2 k_o^2 - \beta^2)^{1/2}$$

$$q = (\beta^2 - n_2^2 k_0^2)^{1/2} \qquad 2.1.8$$

$$p = (\beta^2 - n_3^2 k_0^2)^{1/2}$$

$$k_0 \equiv \frac{\omega}{c}.$$

By imposing the continuity requirement on $\partial \mathbb{E}_y / \partial x$ at $x=-t$, we get from Eq. (2.1.7)

$$h \sin(ht) - q \cos(ht) = p \left[\cos(ht) + \frac{q}{h} \sin(ht) \right],$$

or

$$\tan(ht) = \frac{p + q}{(h - pq/h)} \qquad 2.1.9$$

Equation (2.1.9) is often called the eigenvalue equation meaning that the propagation constant β of a TE mode satisfies this condition.

2.1.3 TM Mode

The field components of TM mode are

$$Hy(x,z,t) = \mathbb{H}y(x)\, e^{i(\omega t - \beta z)}$$

$$Ex(x,z,t) = \frac{i}{\beta\varepsilon} \frac{\partial Hy}{\partial z} = \frac{i}{\omega\varepsilon} \mathbb{H}y(x)\, e^{i(\omega t - \beta z)} \qquad 2.1.10$$

$$Ez(x,z,t) = - \frac{i}{\omega\varepsilon} \frac{\partial Hy}{\partial x}$$

the mode function is taken as

$$\mathbb{H}y(x) = \begin{cases} -c \left[\frac{h}{q} \cos(ht) + \sin(ht) \right] e^{p(x+t)} & x<-t \\ c \left[- \frac{h}{q} \cos(hx) + \sin(hx) \right] & -t<x<0 \\ -c \frac{h}{q} e^{-qx} & 0<x \end{cases} \qquad 2.1.10$$

The continuity of Hy and Ez at the two interface leads to the eigenvalue equation[8]

$$\tan ht = \frac{p(\underline{p} + \underline{q})}{h^2 - \underline{p}\,\underline{q}} \qquad 2.1.11$$

where

$$\underline{p} = \frac{n_2^2}{n_3^2} p , \qquad \underline{q} = \frac{n_2^2}{n_1^2} q.$$

2.2 Effective Dielectric Function Calculation

We consider the case of microparticles of semiconductor (guest) embedded between two layers of PMMA film(host). The size of the microparticles is much smaller than the optical wavelength used when an optical wave propagation in such structure dielectric waveguide is affected by the induced electric and magnetic dipoles in the dielectric. R.E.Collin[9] used Lorentz theory to solve the dipole terms in the induced field. The induce dipole moment is

$$p = \alpha_e \varepsilon \ (E_o + E_i) \qquad 2.2.1$$

α_e :the electrical polarizability of a conducting particle,

ε :the host material permittivity,

E_o :the external field,

E_i :the interactive field between the induced dipole.

The total polarization of suspended particles in the polymer is

$$\mathbb{P} = N \alpha_e \ \varepsilon \ (E_o + E_i) \qquad 2.2.2$$

N : the number density of electric dipoles,

also

$$E_i = \frac{C\,p}{\varepsilon} \qquad 2.2.3$$

C : coupling constant between the dipoles.

Substituting Eq.(2.2.3) into Eqs.(2.2.1) and (2.2.2), we get

$$p = \frac{\alpha_e \varepsilon E_o}{1 - \alpha_e C} \qquad 2.2.4a$$

$$\mathbb{P} = \frac{N \alpha_e \varepsilon E_o}{1 - \alpha_e C} \qquad 2.2.4b$$

The average displacement flux is defined by

$$D_a = \varepsilon E_a + \mathbb{P} = \varepsilon_{eff} E_a \qquad 2.2.5$$

E_a : the average value of the total field in the medium,

ε_{eff} : effective permittivity.

so

$$\varepsilon_{eff} = \varepsilon + \frac{\mathbb{P}}{E_a} = + \frac{\mathbb{P}}{E_o + E_{pa}} \qquad 2.2.6$$

E_{pa} : the average dipole field produced by all the particles.

The dipole field produced by all particles can be expressed by Fourier series

$$E_p = - \sum_{l=1}^{\infty} \sum_{m=1}^{\infty} \sum_{n=1}^{\infty} A_{lmn} \frac{2m\pi}{b} \cos(\frac{2l\pi}{a}x)\cos(\frac{2m\pi}{b}y)\cos(\frac{2n\pi}{c}z) \qquad 2.2.7$$

it is clear from Eq.(2.2.7) that the average induce field is zero since cosine terms have a zero average.

Substituting $E_{pa} = 0$ into Eq.(2.2.6), we get

$$\varepsilon_{eff} = \varepsilon \left(1 + \frac{N \alpha_e}{1 - \alpha_e C} \right) \qquad 2.2.8$$

In the same manner as above, we can get effective permeability

$$\mu_{eff} = \mu \left(1 + \frac{N \alpha_m}{1 - \alpha_m C} \right) \qquad 2.2.9$$

α_m : the magnetic polarizability of a conducting particle,

C : interaction constant between the magnetic dipoles.

H.Grebel and P.Chen[10] have reported that when a dielectric waveguide is illuminated by a light source having a photon energy above the semiconductor band gap and excite the free carriers in the semiconductor clusters are excited. These carriers effectively introduce a transverse interface for light propagating in the slab waveguide with a photon energy smaller than the semiconductor band gap. The short lifetime of the carriers will create electric dipoles, i.e, an increase the permittivity constant. When shielding current is effectively suppressed owing to surface states, there may not be a change in the permeability constant.

CHAPTER 3 PRINCIPLES OF THIN FILM DEPOSITION

3.1 Introduction

Two different film deposition techniques were used in this study. One is plasma polymerization of PMMA; another is vapor deposition of CdS. Below a short introduction to the theory of both techniques is given.

3.2 Plasma Polymerization

The starting material for plasma polymerization is called monomer. When the vapor monomer is introduced into the vacuum chamber, an electrical discharge occurs between two electrode plates. The discharge causes an ionization and fragmentation of the monomers and a subsequent rebonding the fragments into a much larger structure.

H. Yasuda[11] have published a book called " Plasma Polymerization " which is a very good reference for the theory of the plasma polymerization process The factors that affect the deposition rate in the plasma polymerization are :(1) type of electric supply, (2) arrangement of substrates[12], (3) gas pressure[13], (4)monomer flow

rate[14], (5) discharge current and field[15], (7) carrier gas (i.e. He, Ar, N_2, H_2.)[16]. The process can be carried out with ac or dc current. In ac discharge, rf source (13.56 MHz) is typically used, but the power source at 60 Hz is also common. The voltage and current of dc discharge are typically 200 V and 0.1 ~ 1 mA. Gas pressure in the discharge is typically from 0.1 to 10 mtorr.

3.3 Evaporation and Nucleation

3.3.1 Evaporation Processes

Deposition processes consist of three major steps[17]:

1. Generation of the depositing species.

This is a transition from the condensed phase to the vapor phase, The vapor species are generated by heating the material to be evaporated using resistance, induction, electron beam or laser beam heating sources.

2. Transport of the species from the source to the substrate.

This can be in the form of molecular or viscous flow .The mean free path of molecular flow is larger than the source-to-substrate distance and molecular flow occurs at low partial pressures of the depositing species and residual gas in the system. Viscous flow occurs at high partial pressure 20 - 120 mtorr. It also occurs when a substantial partial pressure of an inert gas is intentionally added in the evaporation deposition process to cause gas-scattering of the

deposition species.

3.Film growth on the substrate.

The process depends on the energy of incident species and substrate temperature. Ions and neutrals bombarding the growing film influence the structure, composition, and residual stress of the film.

3.3.2 Mechanism of Film Growth

The general picture of the sequence of the nucleation and growth steps to form a continuous film which emerges from nucleation theory and electron-microscopic observations is described in the "Handbook of Thin Film Technology "[18] as follows:

1. Formation of absorbed monomers.

2. Formation of subcritical embryos of various sizes.

3. Formation of critically sized nuclei (nucleation step).

4. Growth of these nuclei to supercritical dimensions with the resulting depletion of monomers in the capture zone around them .

5. Concurrent with step 4, there will be nucleation of critical clusters in areas not depleted of monomers.

6. Clusters touch and coalesce to form a new island occupying an area smaller than the sum of the original two, thus exposing fresh substrate surface.

7. Monomer adsorbs on these freshly exposed areas, and "secondary" nucleation occurs.

8. Large islands growth together, leaving channels or holes of exposed substrate.

9. The channels or holes fill via secondary nucleation to give a continuous film.

Some of these steps are shown schematically in Fig.4-4. obtained

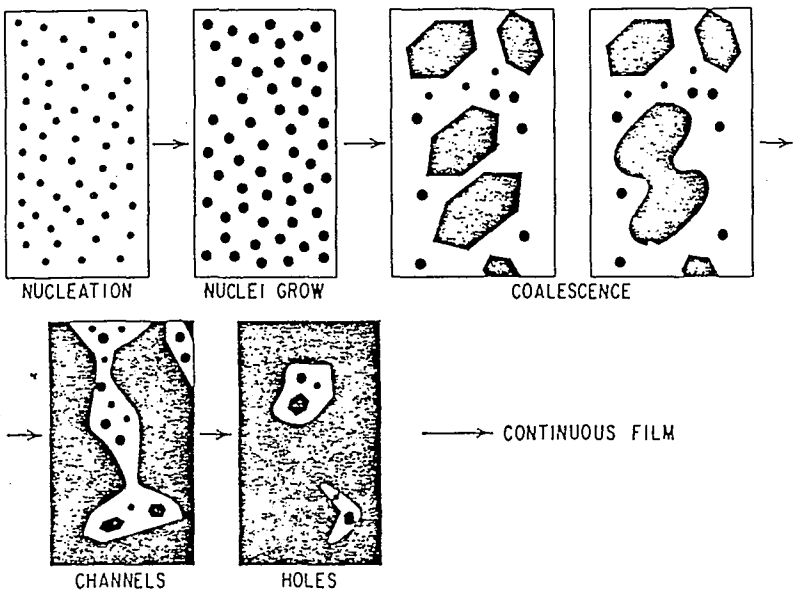

Fig.3-1 Scheme of the shape changes of the film growth.

from reference [18]. It shows the growth process to four stages: nucleation and island structure coalescence of islands, channel formation, and formation of continuous film.

From the above description, it is clear that the film morphology changes with its average thickness. If only a small amount of material is deposited on the substrate it will be present in the form of small clusters or unconnected islands. To obtain a continuous film a minimum average thickness has to be developed. The thickness of which a continues film forms depends on a number of factors such as the

depended material used, surface condensation, surface temperature, surface preparation and deposition rate.

CHAPTER 4 APPARATUS FOR THIN FILM DEPOSITION

4.1 High Vacuum Evaporator

4.1.1 Vacuum Chamber

The vacuum chamber used for evaporation of cadmium sulfide consists of a Pyrex bell jar and gasket resting on a stainless steel base plate assembly. The stainless steel base plate has a cylinder welded below it which contains a main valve and an LN2 cooled baffle to which the diffusion pump is bolted. Six low voltage high current feedthroughs are located in the base plate. The feedthrough supports a fixture for the evaporation source and accessories.

The vacuum gauging includes two Hastings thermocouple gauges. A selector switch at the controller panel allows to read pressures down to one militorr at the mechanical pump (TC-1) or in the bell jar (TC-2).

The Cold cathode ionization gauge provides reliable pressure measurement in the high vacuum range of 10^{-3} to 10^{-7} torr. The cold cathode ionization gauge is also called Phillips gauge, Pennig gauge,

or Discharge gauge. Pressure is determined by measuring the ion current caused by collisions between gas molecules and electrons. A magnet causes the electron to follow long helical paths which increase the probability of gas collisions and result in greater sensitivity at low pressure.

4.1.2 Evaporation Source

The evaporation source consists of a BN crucible (1.3 cm high and 1 cm diameter) containing the material to be evaporated, and a filament. A substrate holder has a form of an aluminum plate(20 × 9 cm^2) with a rectangular hole in the center (15 × 6 cm^2). The distance between the crucible and the substrate holder is 17 cm. The crucible is heated by the filament and the heating temperature is determined by the current supplied to the filament. The whole system structure is shown in Fig.4-1.

4.2 Plasma Generator

4.2.1 Vacuum Chamber and Pumping System

The vacuum system used for PMMA polymerization consists of a Pyrex tube (45 cm high and 15 cm diameter), top and bottom flanges, valves, a vapour trap, a mechanical pump and a diffusion pump.

The monomer flow control system consists of a high vacuum valve,

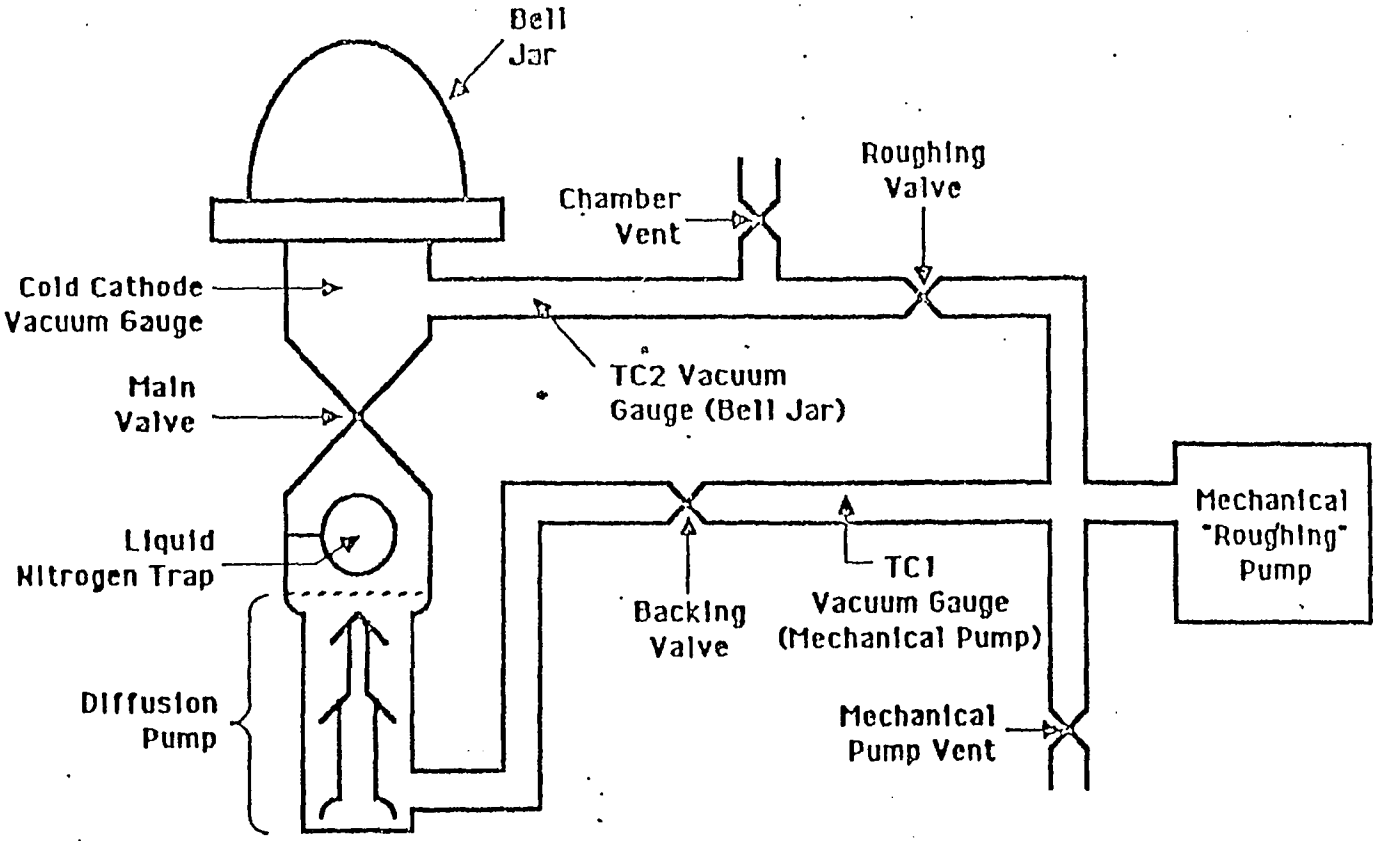

Fig. 4-1. High vacuum evaporator

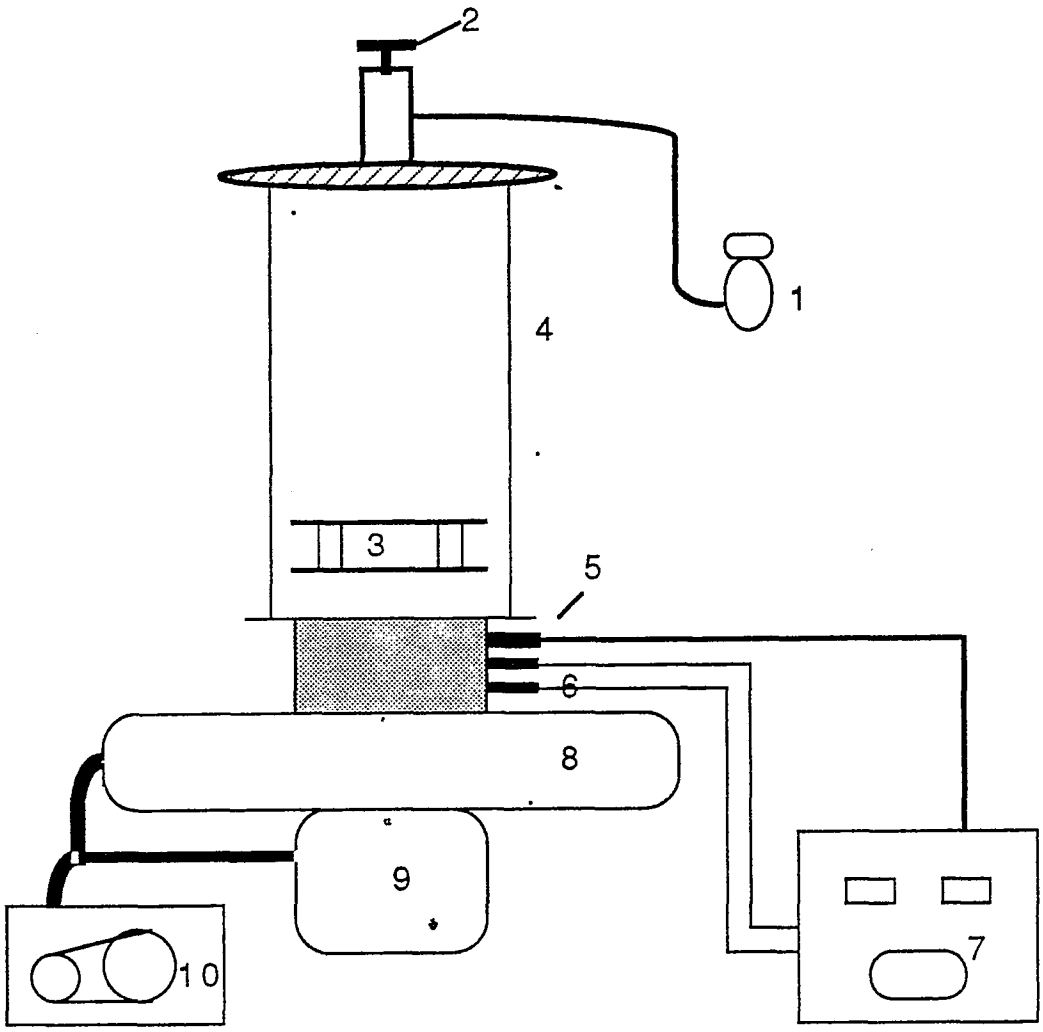

1.vessel for liquid monormer

2 micronmeter

3.electrode plates

4 Pyrex bell jar

5 thermalcouple gauge

6 voltage input

7 electrical control system

8 vapour trap

9 diffusion pump

10 mechanical pump

Fig. 4-2 plasma deposition system

a micronmeter needle valve (to control the monomer flow rate) and a vessel containing liquid monomer.

4.2.2 Electrical System

Plasma discharge occurs between two rectangular electrode plates (11.5 × 6.5 cm^2).The distance between the two electrode plates is 3.2 cm. The ac voltage (60 Hz) was supplied between two electrode plates . The voltage and the current of the discharge measured by the meters on the control panel. The panel also contains a process timer. The plasma generator is shown in Fig.4-2 and the electrical system is shown in Fig.4-3.

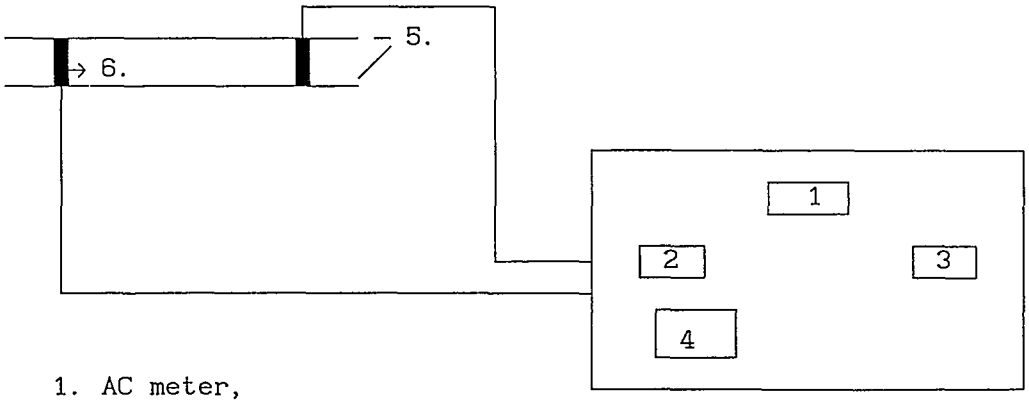

1. AC meter,
2. Output current meter,
3. Input current meter,
4. Timer,
5. Electrode plates,
6. Insulator.

Fig.4-3 Electrical system.

CHAPTER 5 EXPERIMENT

5.1 Waveguide Fabrication Method

5.1.1 Starting Materials

1. Waveguide host material:dehibited methyl-methacrylate monomer liquid.

2. Guest material: Cadmium sulfide (CdS),powder.

3. Substrate. microscope slide glass, 26mm x 76mm.

5.1.2 Procedure

A. Plasma deposition:

1. Load the vessel with liquid monomer and place substrates (typical 3) between two electrodes.

2. Start to pump the plasma deposition system using mechanical pump untill the pressure inside the chamber is about 5-10 mtorr.

3. Open the micronmeter of the needle valve to control the pressure inside the chamber and to adjust the flow rate of the monomer. The pressure in the chamber during deposition was set at 300

mtorr.

4. Turn on the power supply and adjust the power of plasma discharge. The voltage across the electrodes was 430 volts and the current 5.4 mA.

5. Deposition time depends on how thick the film is desired. It was typically 45-60 minutes for 2μm thick polymer film.

6. Turn off the power supply, close the roughing valve and turn off the pump.

7. Wait about 30 minutes to let the substrates cool down then take them out.

B. Vapor deposition:

1. Load the crucible with CdS and place the substrate which is prepared by the previous processes (PMMA + glass) on the substrate holder.

2. Pump the evaporator till the pressure is about 4×10^{-6}~ 5×10^{-6}mtorr.

3. Turn on the filament power and adjust the filament current to obtain the desired temperature of the crucible. The temperature was measured using an optical pyrometer and set at 1100 °c. The filament current was 46 A.

4. Deposition time depends on the desired film thickness. It ranged typically from 2 to 3 minutes.

5. Turn off the filament power.

6. Wait for the film cool down

C. Repeat part A (plasma deposition) steps 1-7. to obtain the film as shown in Fig. 1-1.

5.2 Results of Deposition

5.2.1 Deposition Rate of Plasma Polymerization

In this experiment, we investigated the relation between time, pressure and the deposition rate. The results showed that deposition will saturate after a certain time, which may be explained by the fact that the plasma etches the film. Table 5-1 and Table 5-2 list time and pressure related to the film thickness respectively. Also see Fig. 5.1, and Fig. 5.2. which show the results in a graphical form. The film thickness was obtained by measuring the intensity profile width of the waveguide output and dividing it by the magnification factor.

Table 5-1 Variation of PMMA Film Thickness with Time

Time(mins)	Power(w)	Film Thickness(μm)
30	2.322	1.388
60	2.322	2.181
90	2.322	2.026
120	2.322	1.780
180	2.322	1.636

Table 5-2 Variation of PMMA Film Thickness with Pressure

Pressure (mtorr)	Time (mins)	Film thickness (μm)
200	45	1.408
300	45	1.503
400	45	1.522
500	45	1.585
600	45	1.649

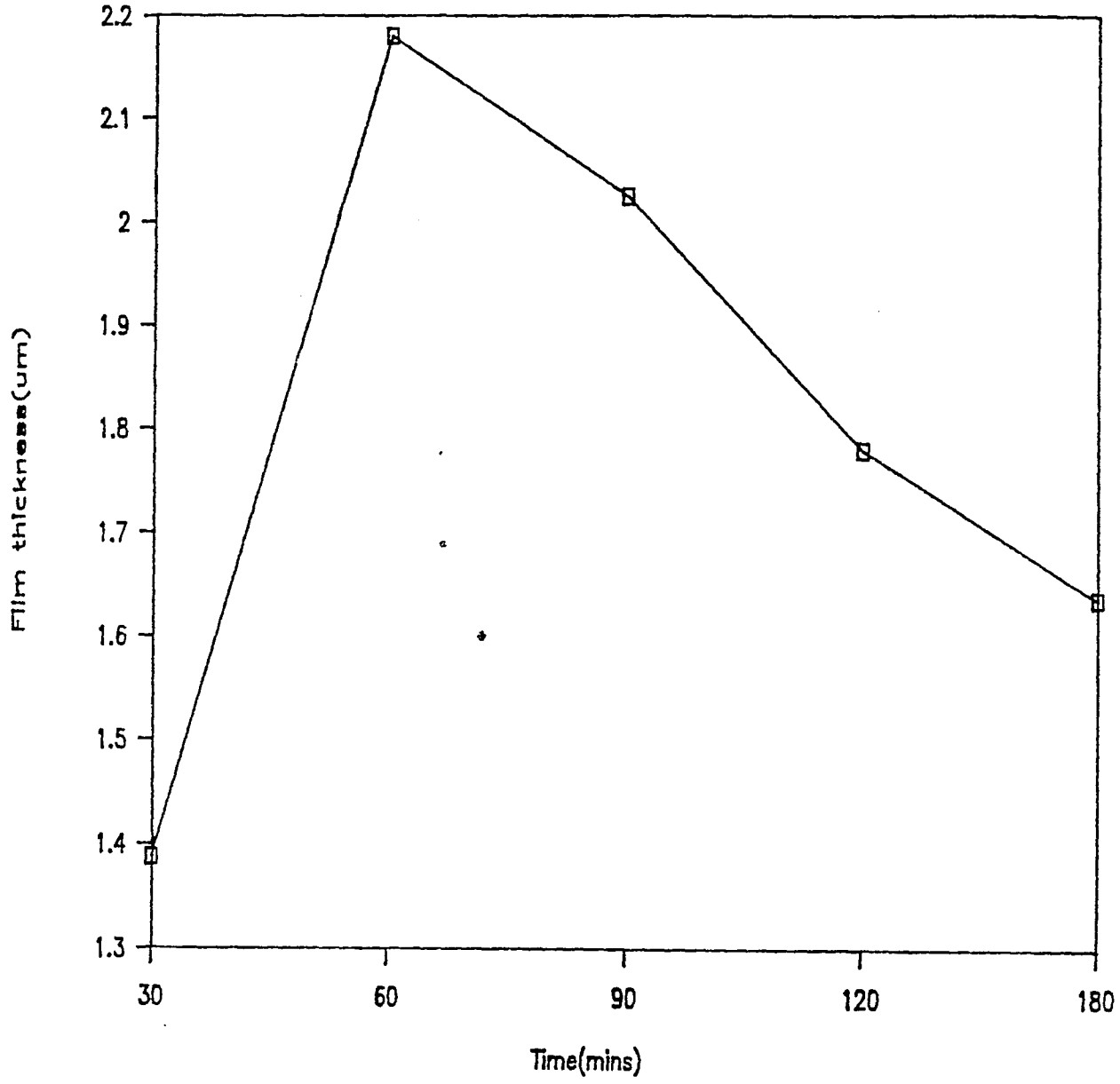

Fig.5-1. Variation of PMMA film thickness with time

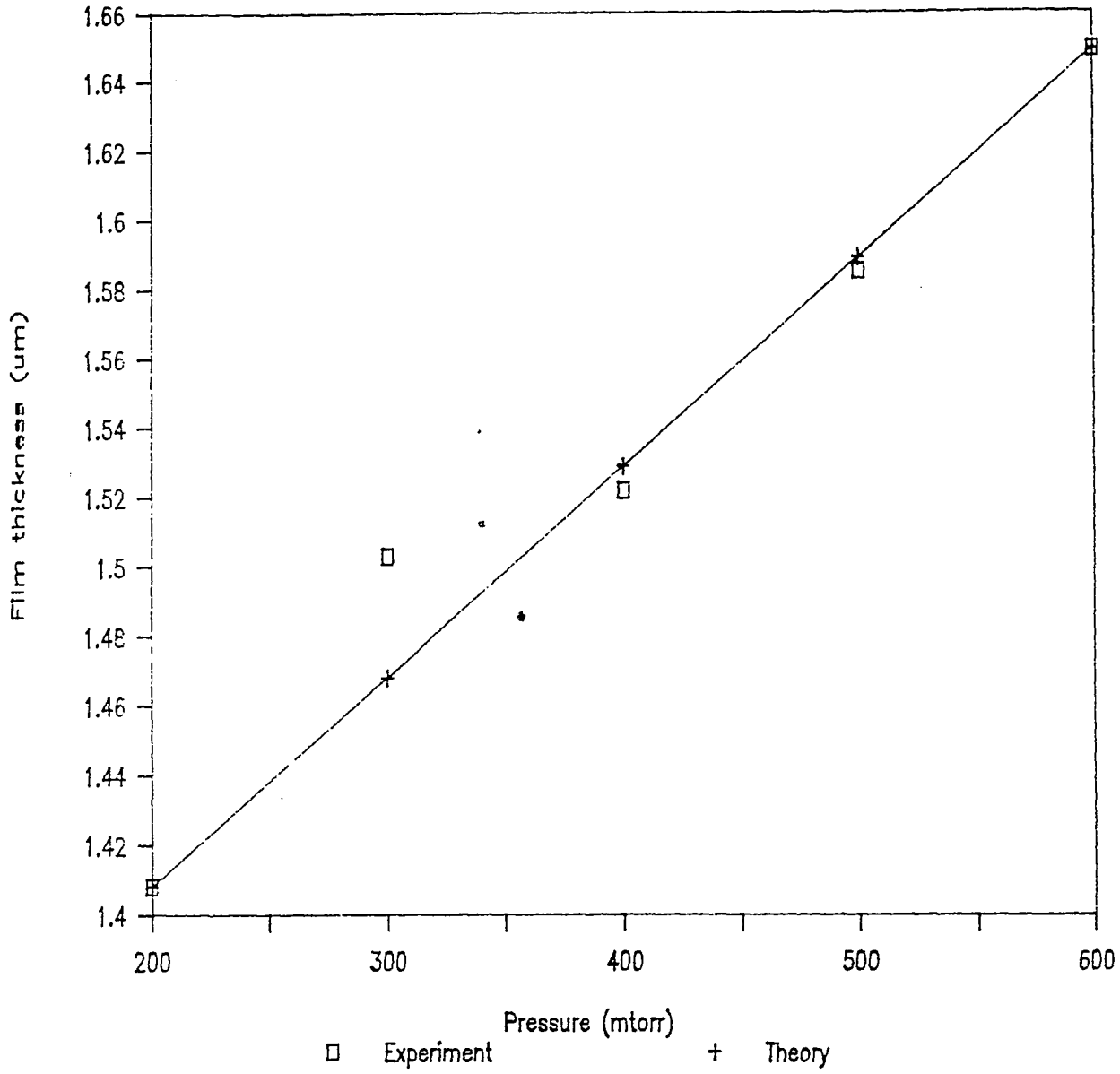

Fig.5-2. Variation of PMMA film thickness with pressure

5.2.2 SEM Measurement

In this experiment, we wanted to get a discontinuous CdS deposit embedded on PMMA films. We kept filament current constant and used deposition time to control the film thickness. Two samples were made at same time, one was brought to the plasma generator to deposit another PMMA film on top of CdS, the other was used to measure the cluster size of CdS by SEM (Scanning Electron Microscope)

SEM samples are prepared as follows:

1. Cut the glass substrate to 1×1 cm^2.

2. Put a little silver paint on the top of SEM holder (cylinder, diameter ~ 1 cm, high ~ 1.5 cm) and place the sample on it.

3. Evaporate a very thin gold film on the sample surface in a vacuum chamber.

The SEM images are shown in **Fig.5.3**. The magnification is 5,000. In the pictures we can see some clusters; their size range from 600Å to 1000Å . The cluster size is smaller than seen in the pictures, because we have to account for the gold film thickness which is estimated to be about 100 Å. We assume the high of the cluster is same as that shown in the SEM image, so the average thickness of the clusters is about 20 Å. The area of the film covered by the clusters is only 0.3 % of the total film area.

The SEM image of pure PMMA shows that the only particles on the

substrate are some dust particles, and their size is about 10 μm. The picture of the PMMA film are shown in Fig.5-4.

5.2.3 RBS Measurement

RBS (Rutherford Backscattering Spectrometry) is a technique for surface analysis. It is used to analyze (1) composition and thickness of thin films, (2) surface impurities, (3) depth concentration distributions in bulk material.

The basic principle of RBS is that a high energy ion beam(2 Mev He^+ in our case)from a Van de Graff accelerator impinges on the sample surface and a solid-state detector receive the back scattered ion. The energy spectrum of the ions is obtained with a multichannel pulse amplitude analyzer.

For calibration purpose, we measured a spectrum of a Si sample and compared to the spectrum of CdS. The spectra of the samples are shown in Fig.5-5, Fig.5-6. The peak between channels 400 and 430 in the spectrum in Fig.5-5 corresponds to the He^+ scattering from Cd. The broad peak between channels 230 and 280 in Fig.5-6 corresponds to He^+ scattering from Si. The number of scattered ions can be expressed as :

$$C = N\ Q\ \sigma\ \Omega \qquad 5\text{-}1$$

C: counts,

N: atomic surface density,

σ: cross-section for coulomb scattering,

Ω: solid angle of detection,

Q: to total charge accumulated by the ion beam.

so

$$C_{Si} = N_{Si}\ Q_{Si}\ \sigma_{Si}\ \Omega_{Si}$$

$$C_{Cd} = N_{Cd}\ Q_{Cd}\ \sigma_{Cd}\ \Omega_{Cd}$$

$$N_{Cd} = N_{Si}\ \frac{C_{Cd}}{C_{Si}}\ \frac{Q_{Si}}{Q_{Cd}}\ \frac{\sigma_{Si}}{\sigma_{Cd}}$$

The subscripts refer to silicon and cadmium. The sample of Si is a wafer which produces a broad profile in the spectrum. The number of counts in 10 channels of Si peak was measured as C_{Si} = 13304. The He^{+} ions which correspond to these counts were scattered by a layer of Si containing $N_{Si} = 10 \times 45.51 \times 10^{15}$ atom/cm^2. The number of atoms corresponding to one channel of the spectrum is given in special tables used in RBS spectroscopy.

The ratio of the cross-sections for coulomb scatters $\frac{\sigma_{Cd}}{\sigma_{Si}}$ is proportional to the ratio of the atomic number square:

$$\frac{\sigma_{Cd}}{\sigma_{Si}} = \left(\frac{Z_{Cd}}{Z_{Si}}\right)^2 = 11.75$$

Q of 1 and 3 μ coul was chosen for Si and Cd respectively in our measurements. The total counts in the Cd peak was 90000 . So

$$N_{Cd} = 45.51 \times \frac{90000}{13304} \times \frac{1}{3} \times \frac{1}{11.75}$$

$$= 8.74 \times 10^{16} \text{ atom/cm}^2$$

The density of CdS is

$$\frac{4.82\ g/cm^3 \times 6.02 \times 10^{23}\ at/mole}{144.46\ g/mole} = 2.01 \times 10^{22}\ at/cm^3$$

So, the average thickness of the film

$$d = \frac{8.74 \times 10^{16}}{2.01 \times 10^{22}} = 4.35 \times 10^{-6}\ cm = 435\ Å$$

If we assume that the average film thickness is proportional to the deposition time, from the result of RBS measurement, we can estimate the average thickness of the films deposited during different times, as shown in Table 5-3.

Table 5-3 Variation of Average Film Thickness with Time

Deposition time(mins)	Average film thickness(Å)
2	248
3	372
4	497

We made RBS measurement on two CdS on PMMA samples. The deposition times were 2(sample A) and 3.5 (sample B) minutes. The spectrum of sample A showed a broad peak, typical of the charging up of the specimen by the ion beam. It was concluded that the sample was not conducting and therefore the CdS material formed islands rather than continuous film.

From RBS measurement we learned that :

(1). The average thickness of sample B is 435 Å. CdS in the sample form rather uniform film as shown by the width of the peak in the

spectra. The clusters seen in SEM images contain only small amount of material.

(2). Sample A is not conducting and contains islands of CdS material.

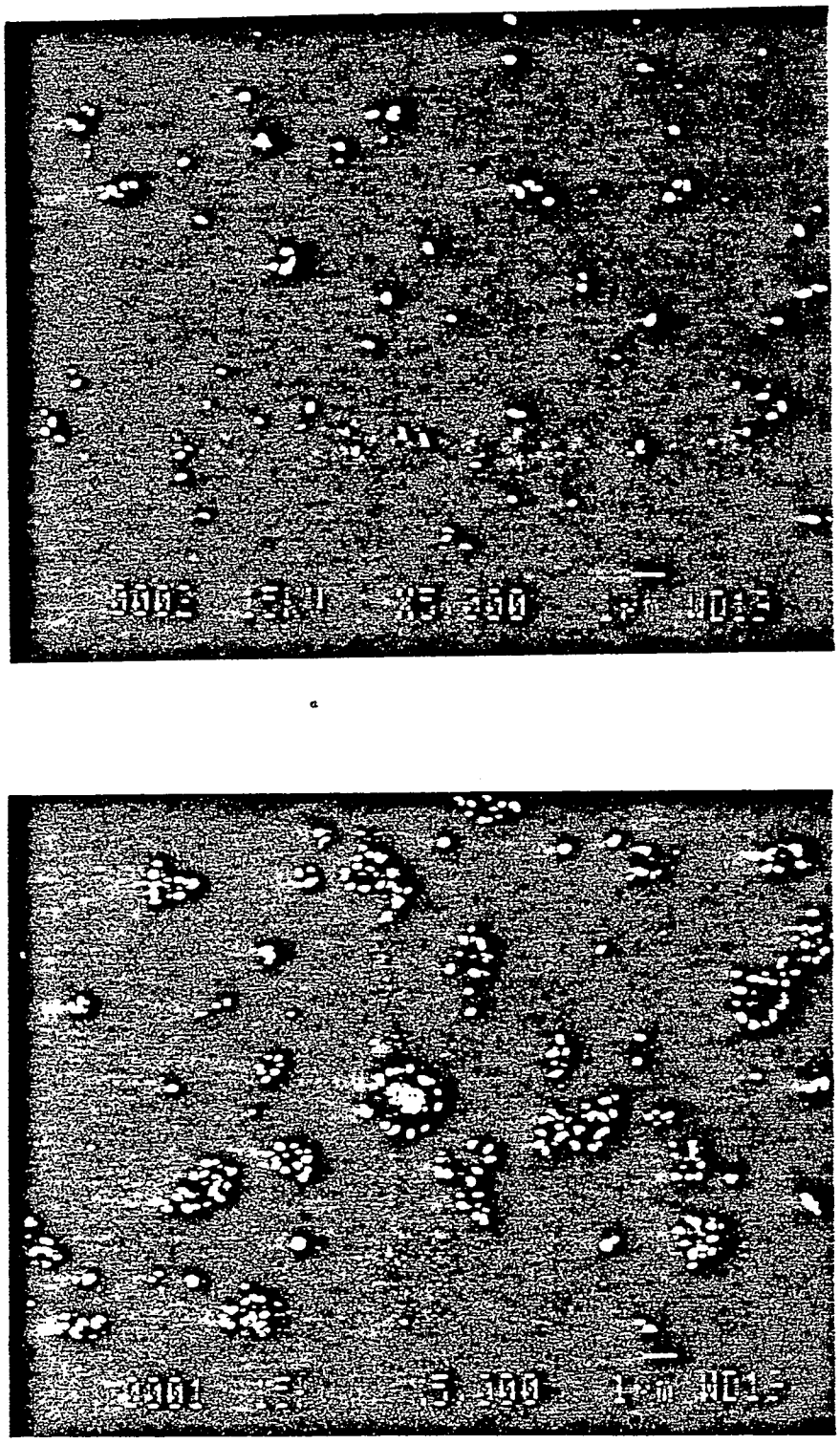

Fig.5-3.SEM image of CdS thin film on PMMA.

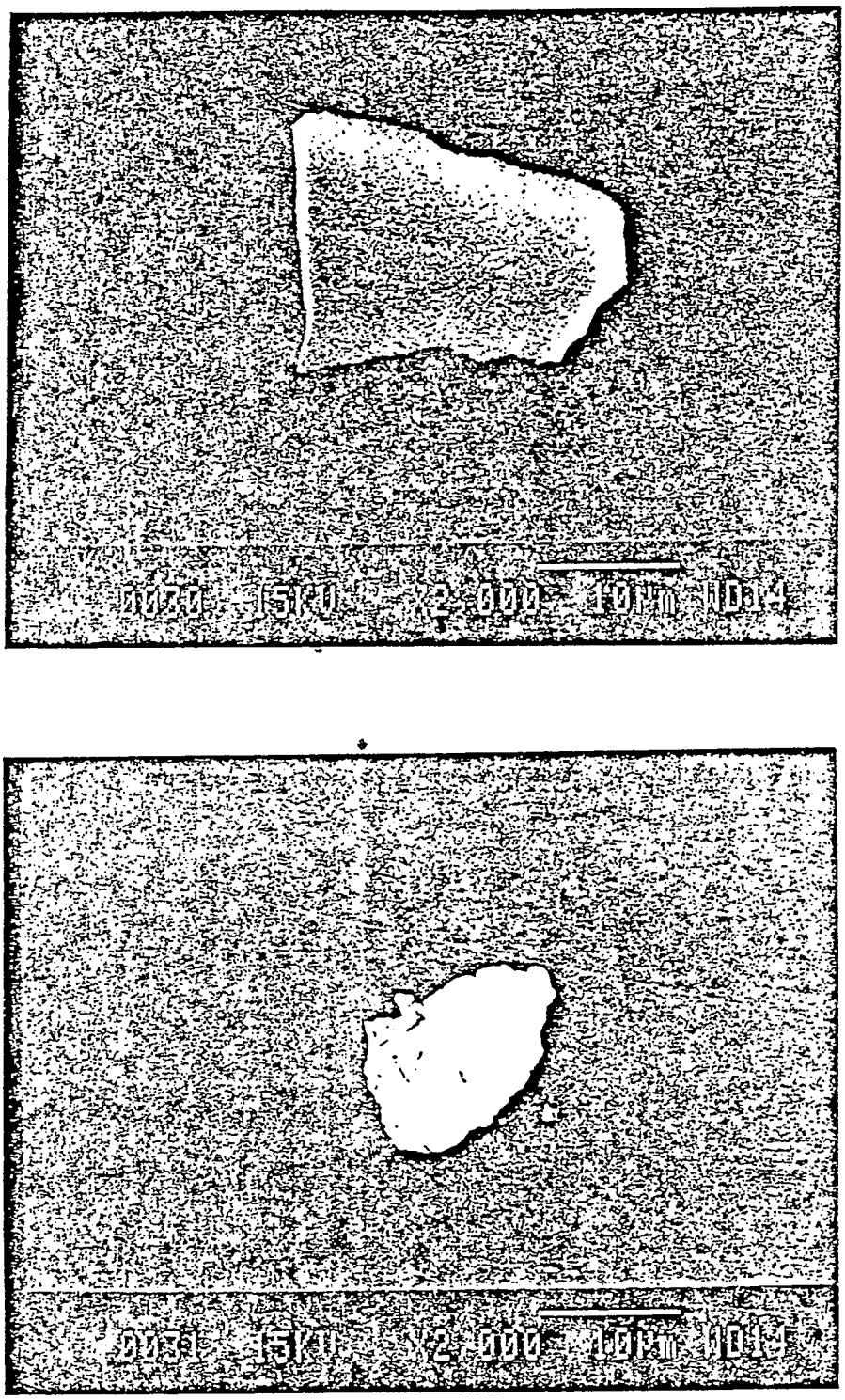

Fig.5-4 SEM image of pure PMMA film

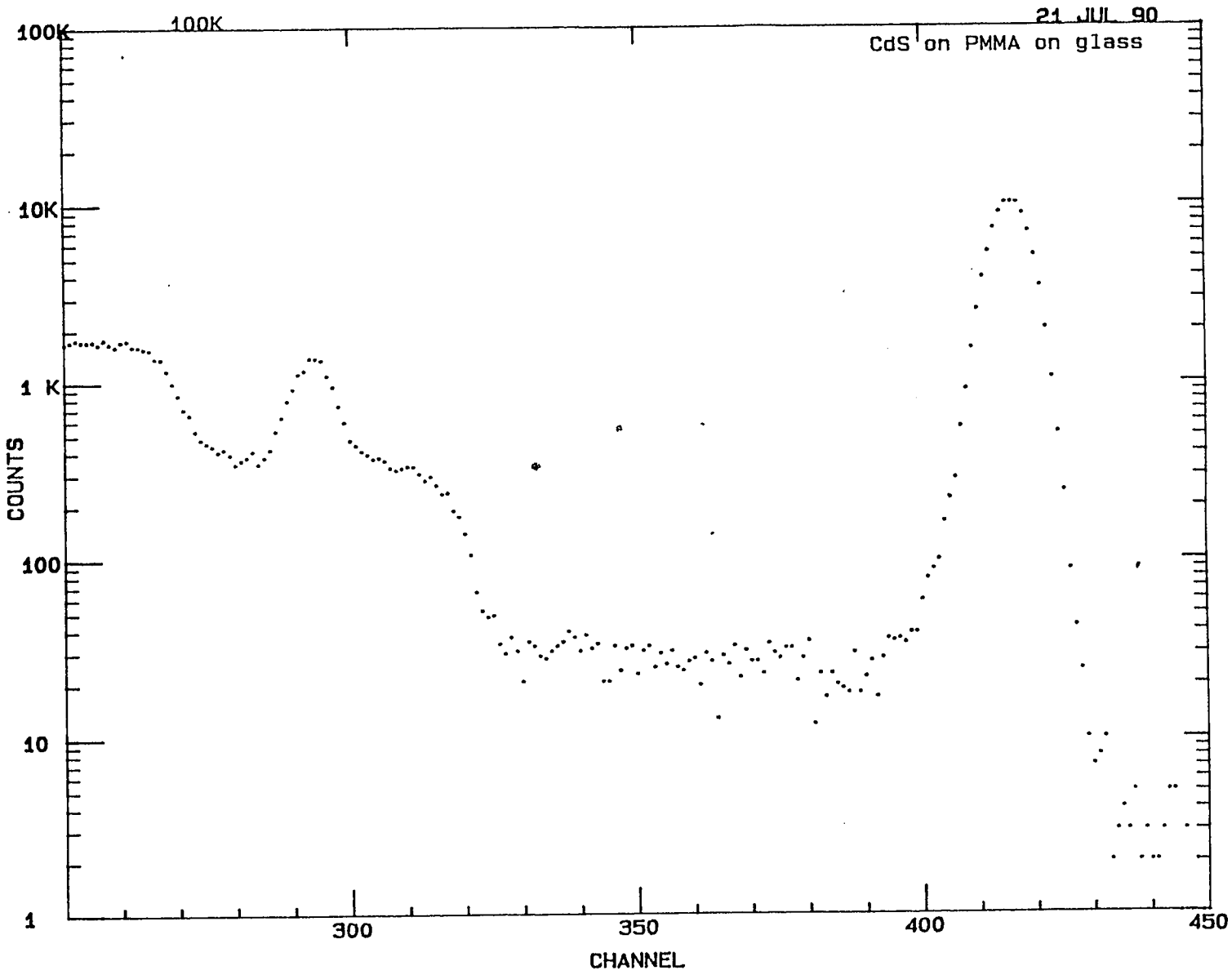

Fig.5-5 The spectrum of CdS

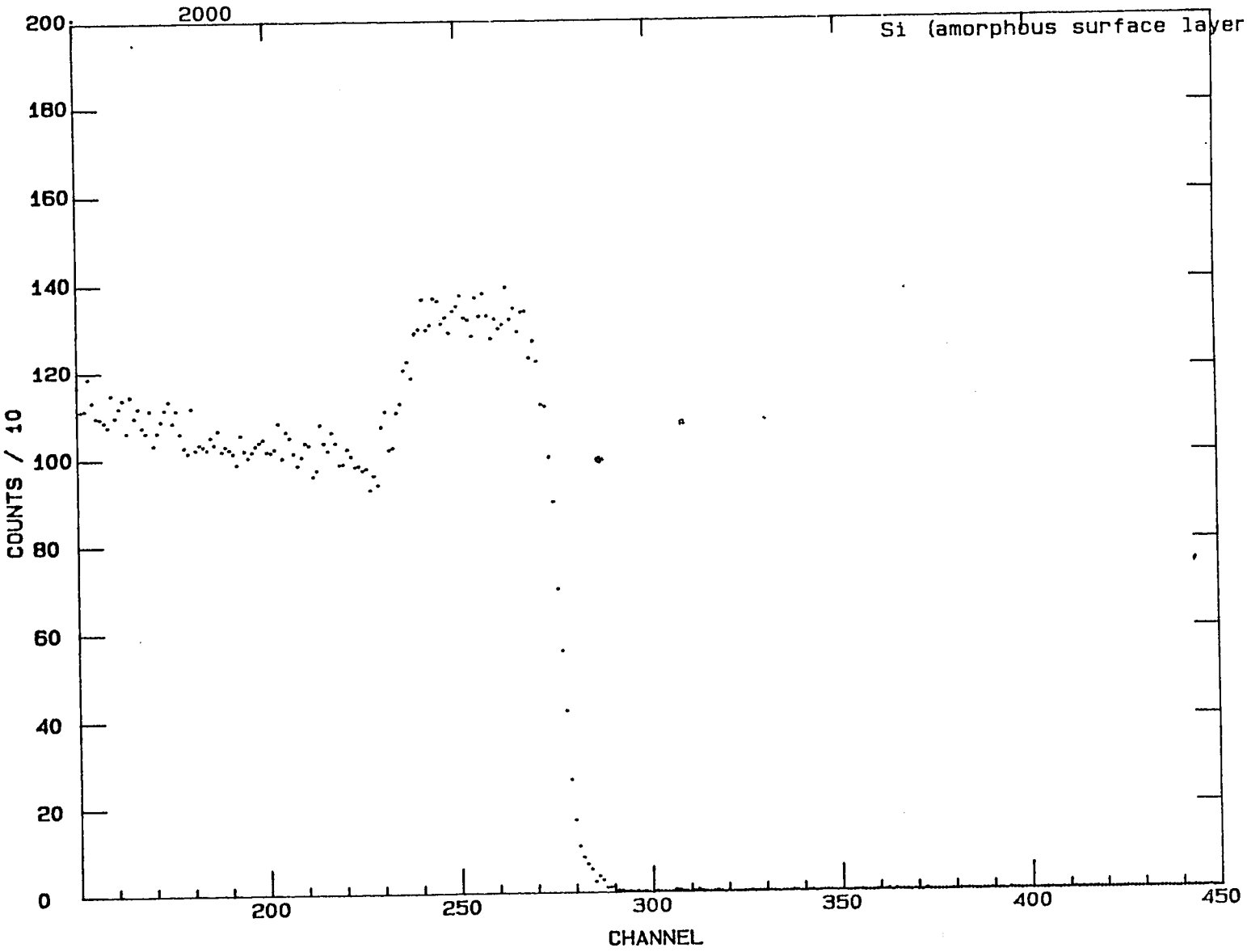

Fig.5-6 The spectrum of Si

5.3 Optical Measurement System

The optical measurement system is shown in **Fig.**5.7 :

1. *Optical chopper* - used with *lock-in amplifier.*

2. *Half - wave plate (Half plate)* - operating on the wavelength of 0.6328 μm, mounted on a rotatable stand. The role of this plate is to switch from one linear polarization mode to another, that is, to enable launching light either to the TE or to the TM modes.

3. *Polarizer 1* - linear polarized filter mounted on a rotatable stand.

4. *Microscope objective 1* (x20) - to focus the laser beam onto the waveguide. The spot size, at the focal point is given by

$$r = 1.22 \cdot \frac{f\lambda}{D}.$$

where r : radius of the spot,

λ : optical wavelength, λ=0.6328 μm,

f : the focal length of the lens used (microscope objective)

D : the diameter of the laser beam.

In the experiment the spot size is approximate 7 μm, larger than the waveguide width.

5. *Microscope objective 2* (x20) - to magnify the near field pattern of the waveguide output.

6. *Photo detector* - to detect the light intensity at the screen, and to send the signal to the *lock-in amplifier.*

7. *Lock-in amplifier* - with a reference frequency provided by the *optical chopper.* The signal from the detector is analyzed and the noise can be reduced to a minimum.

8. *Laser* - He-Ne laser, wavelength λ=0.6328 μm.

9. *HP-300 computer* - to record the data from the *lock-in amplifier.*

10. *Motorizer* - to move the detector in the Y direction with respect to to waveguide axis.

11. *Controller* - to control the speed of motorizer.

12. *Light source* - to illuminate the sample.

13. *Plotter* - connected to *HP-300 computer.*

14. *Waveguide sample*

15. *Filter.* - only red light can pass through the filter to the detector.

The laser light beam which propagates through the optical waveguide is detected by a detector. Because the light intensity is very weak, an *optical chopper* which provide a reference frequency to the *lock-in amplifier* is used to reduce the background noise. The frequency of the *optical chopper* is chosen not to be near the frequency of the power system, 60 Hz or its integer multiplication. The signal, including the background noise from the detector, is sent to the *lock-in amplifier* and by comparing the signal from the detector to the reference frequency from the *optical chopper* , the background noise which is not modulated by the *optical chopper* frequency is reduced to minimum. The output of the *lock-in amplifier* is converted to digital signal and sent through a IEEE-488 interface to the HP-300 computer.

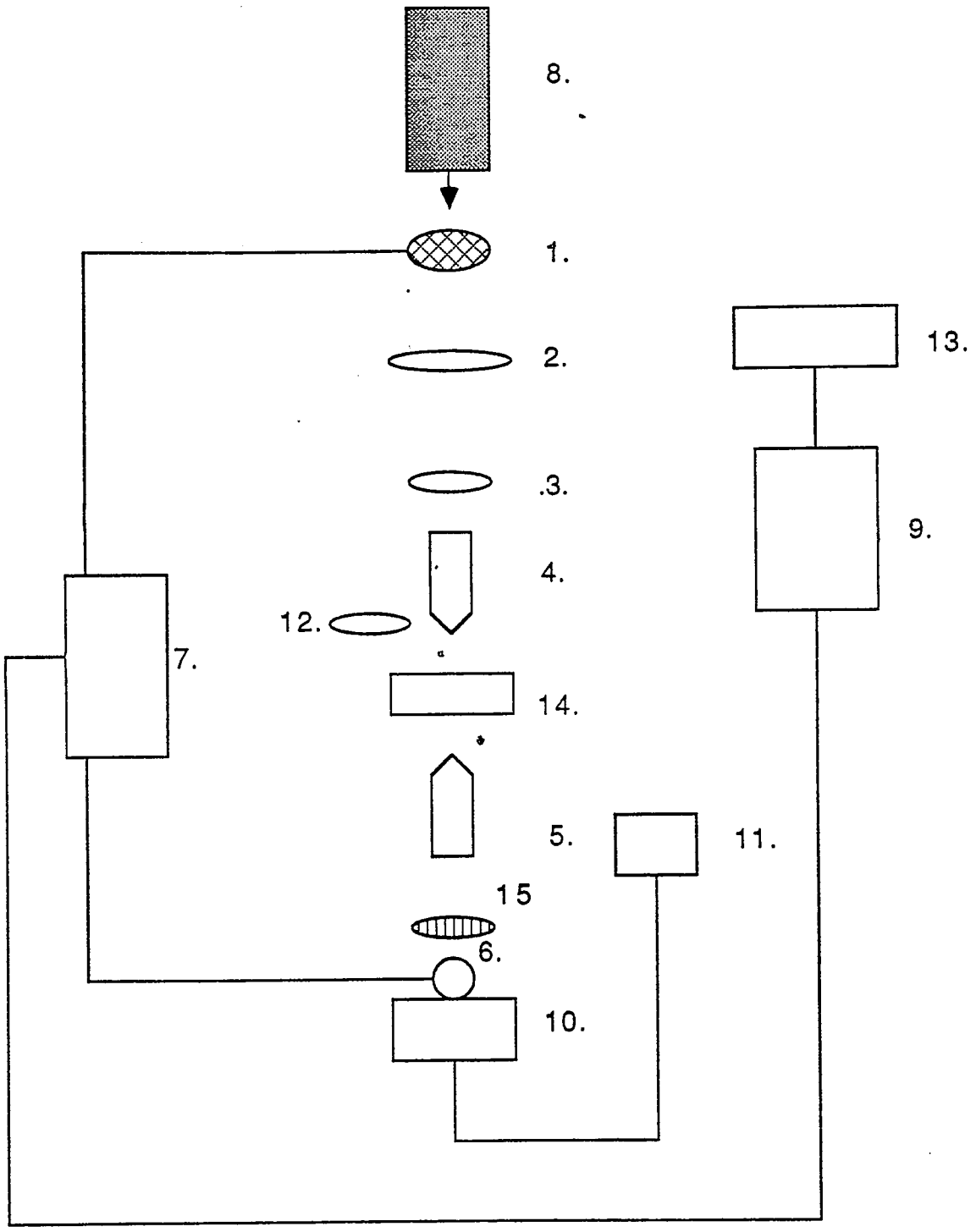

Fig.5-7 The optical measurement system

5.4 Near-Field Pattern Measurement

Near - field measurements are the intensity profile just at waveguide output. In measuring the near-field pattern of TE or TM mode, the waveguide output is magnified by *objective 2*. The image size of the intensity at the detector is about 1mm.

The set up of the near-field pattern measurement is shown in Fig.5-7. A detector with a pin hole to limit the detector aperture size is used to scan over the magnified near-field-pattern. The diameter of the pin hole is about 60~100μm. The pin hole and the detector are mounted together on a motorizer which provides a vertical movement. By scanning the near-field pattern across the waveguide width at the vale of 5.7um/sec, the near-field pattern of the TE or the TM mode is measured.

5.4.1 Measurement Procedure

1. Adjust half plate to proper angle, as observed in Fig.5-7.
2. Adjust the frequency of the optical chopper.
3. Adjust the microscope objective to magnify the near-field pattern of the waveguide and focus the near-field pattern of the waveguide on detector.
4. Adjust the motorizer position.
5. Set the lock-in amplifier phase and time constant.
6. Use HP-300 computer to record the data from the lock-in

amplifier. After a complete measurement the computer will make a sound.

7. Wait for the signal from the computer then turn on the white light source to illuminate the waveguide sample. Record the data again.

8. Wait for the signal from the computer then turn off the white light source.

5.4.2 Experimental Results

In this experiment, we measured several samples, prepared with different deposition time of CdS, under white light illumination. Table 5-4 and Table 5-5 shows the results with the intensities obtained with and without illumination normalized to unity . The intensity difference between the profile might be attributed to scattered light. This is not considered as an inherent property of the waveguide and may be accounted by proper normalization . For example, profiles of a waveguide show the intensity under white light illumination and under no illumination, which are not normalized in Fig.5-8 and Fig.5-9.

Table 5-4 TE mode

T(mins)	Wb-Wa(um)	Fig.No
2	0.296	5.10
3	0.135	5.11
4	0.082	5.12
5	no waveguide detected	

T : deposition time.

W_b: waist of waveguide without light illumination.

W_a: waist of waveguide with light illumination.

W_b-W_a:difference between waist without light and with light illumination.

Table 5-5 TM mode

T(mins)	W_b-W_a(um)	Fig.No
2	0	5.13
3	0.12	5.14
4	- 0.16	5.15
5	no waveguide detected	

Fig.5-10 ~ Fig.5-12 and Fig.5-13 ~ Fig.5-15 were the near-field pattern of the waveguide in TE and TM modes with different deposition time of CdS. From Table.5-4 and Table.5-5, the biggest change of the waist of the waveguide showed in TE mode. In TM mode, we did not find too much change of the waist of the waveguide.

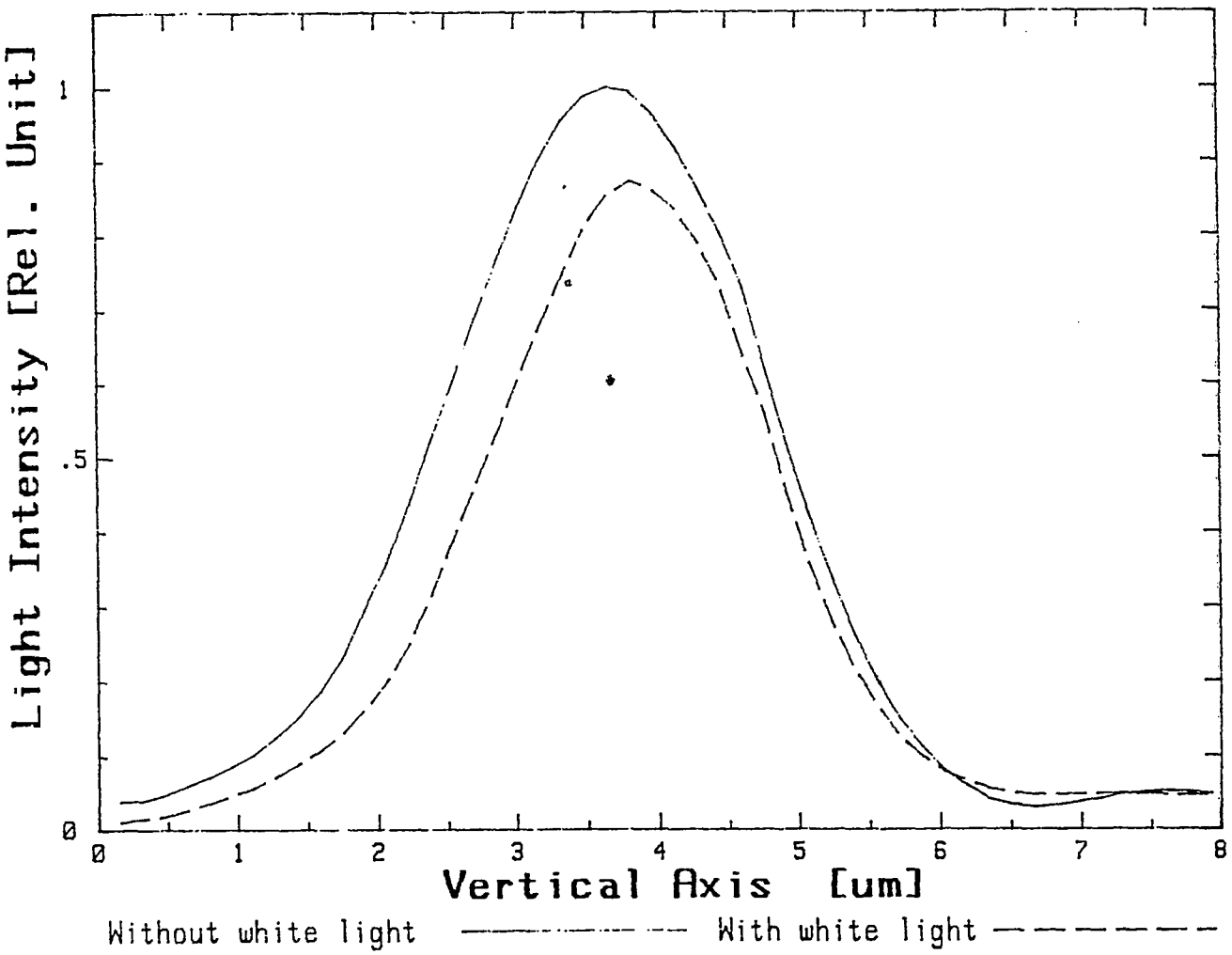

Fig.5-8 The near-field pattern of PMMA-CdS-PMMA waveguide in TE mode

The deposition time of CdS is 3 minutes.

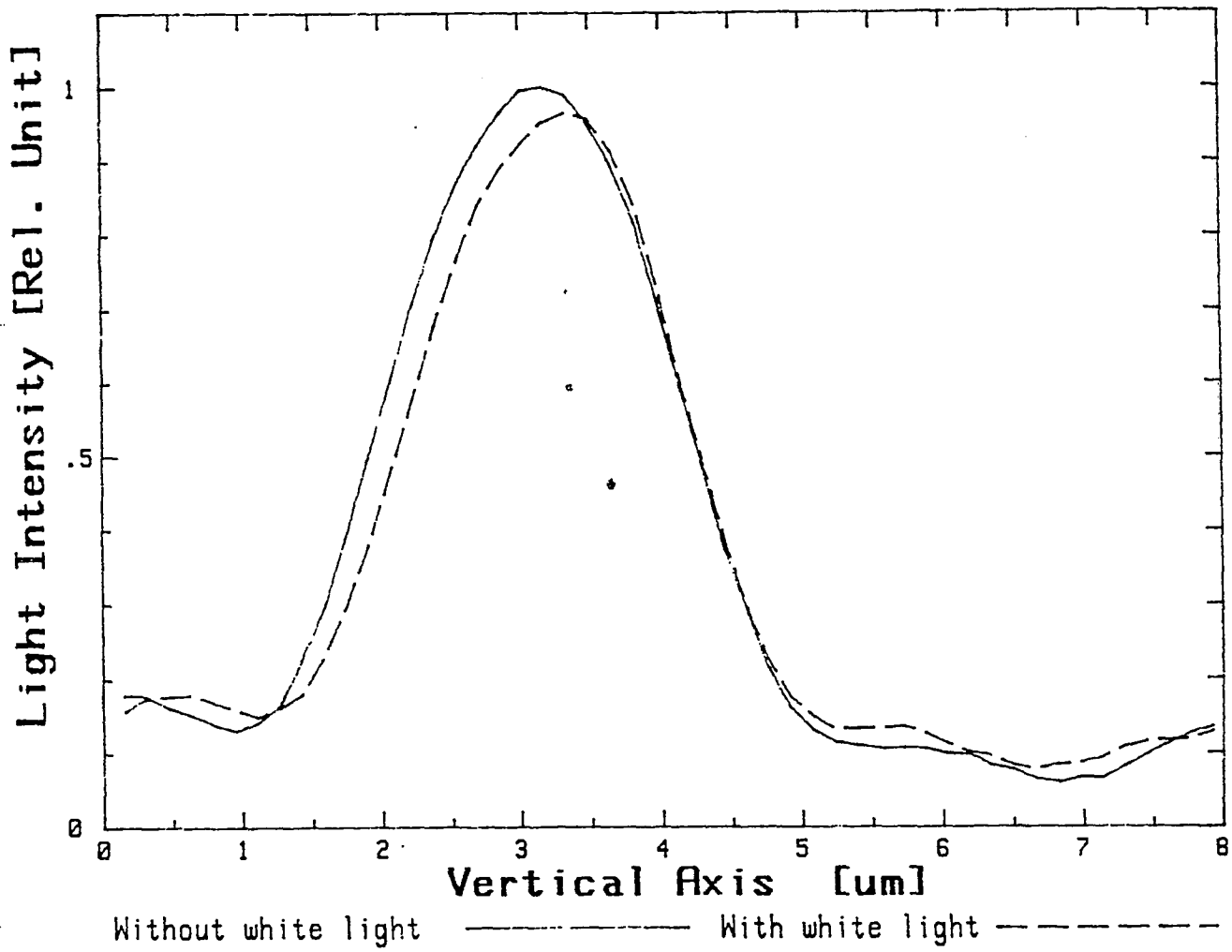

Fig.5-9. The near-field pattern of PMMA-CdS-PMMA waveguide in TM mode

The deposition time of CdS is 3 minutes.

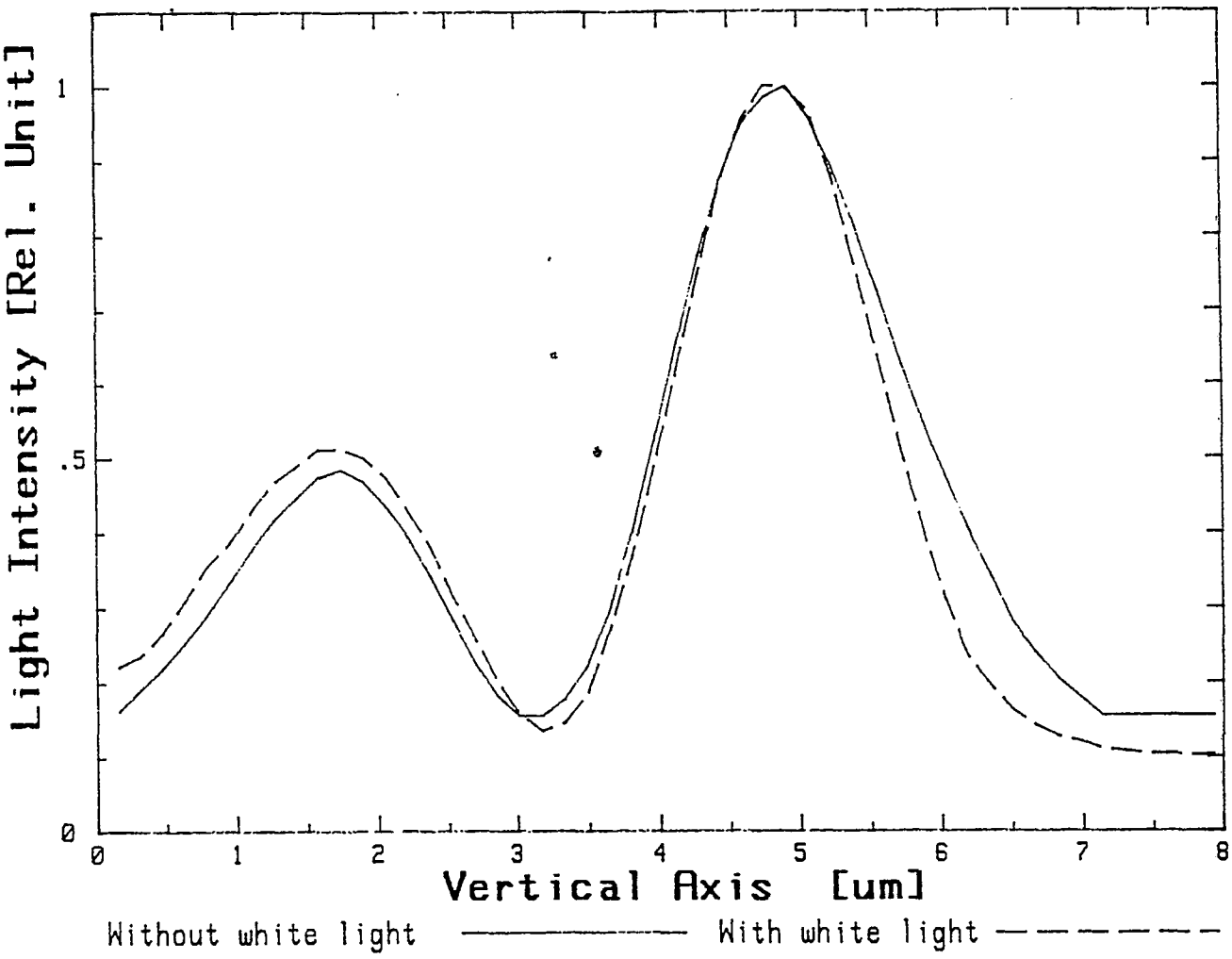

Fig.5-10. The near-field pattern of PMMA-CdS-PMMA waveguide in TE mode. The deposition time of CdS is 2 minutes.

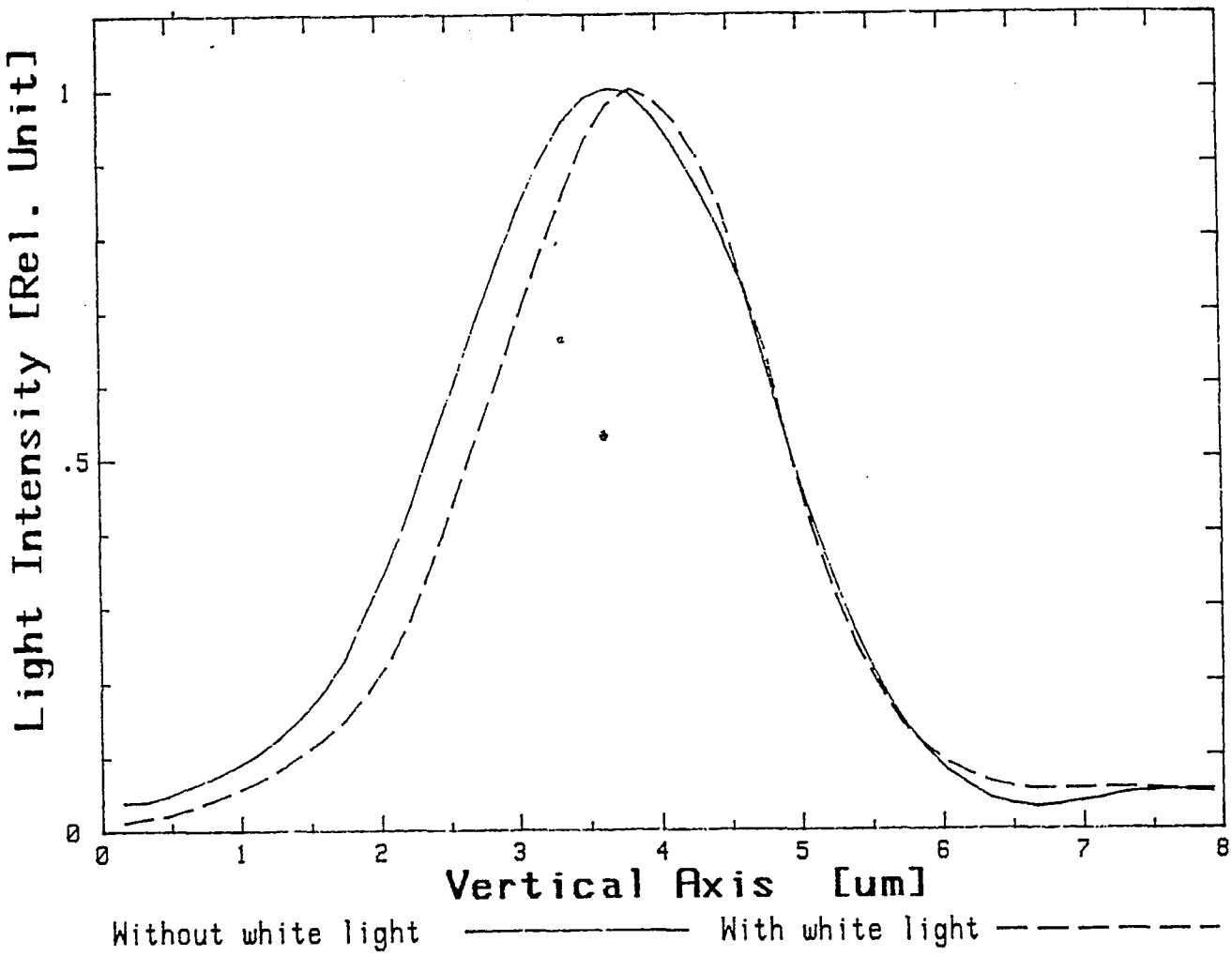

Fig.5-11. The near-field pattern of PMMA-CdS-PMMA waveguide in TE mode. The deposition time of CdS is 3 minutes.

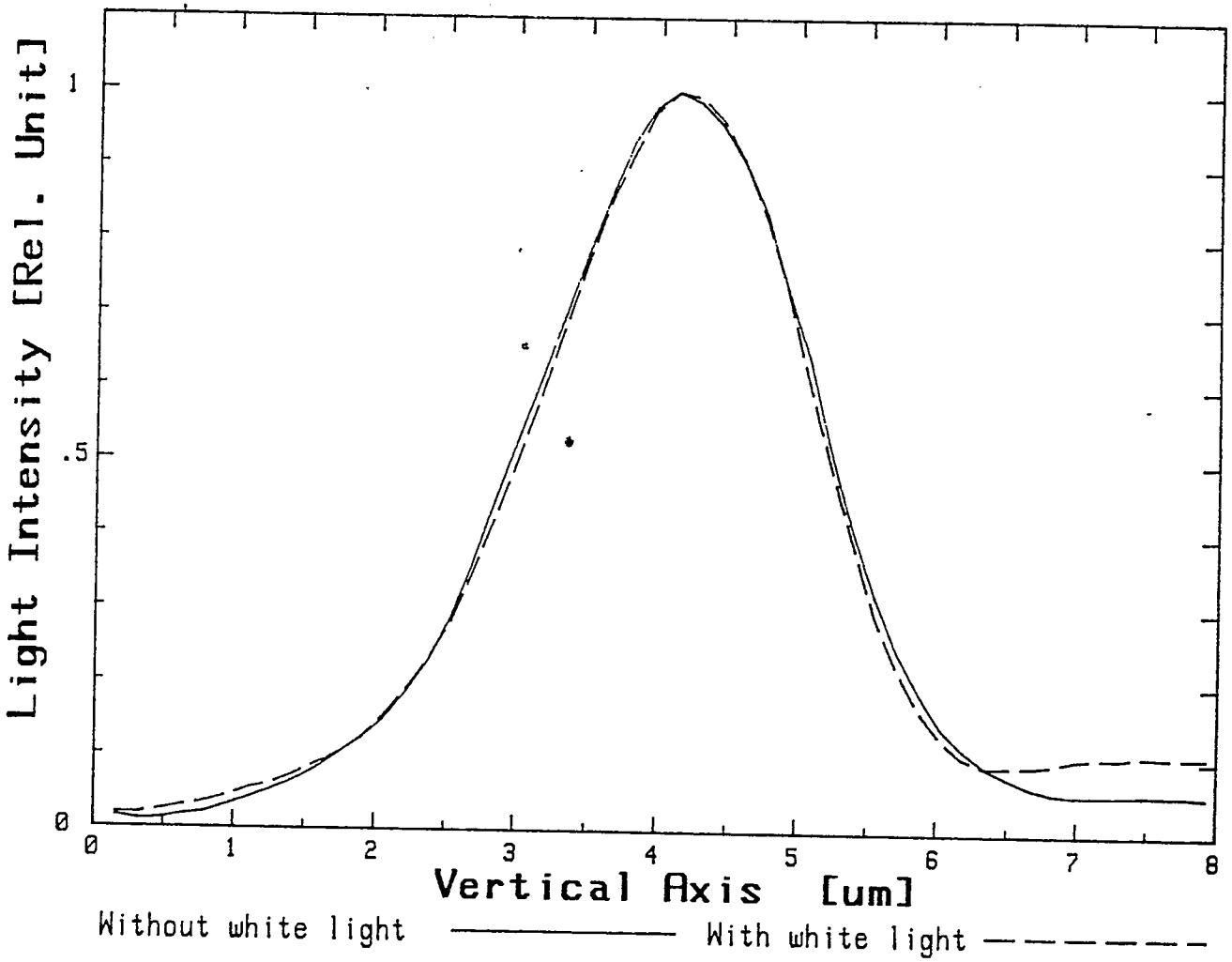

Fig.5-12. The near-field pattern of PMMA-CdS-PMMA waveguide in TE mode

The deposition time of CdS is 4 mins

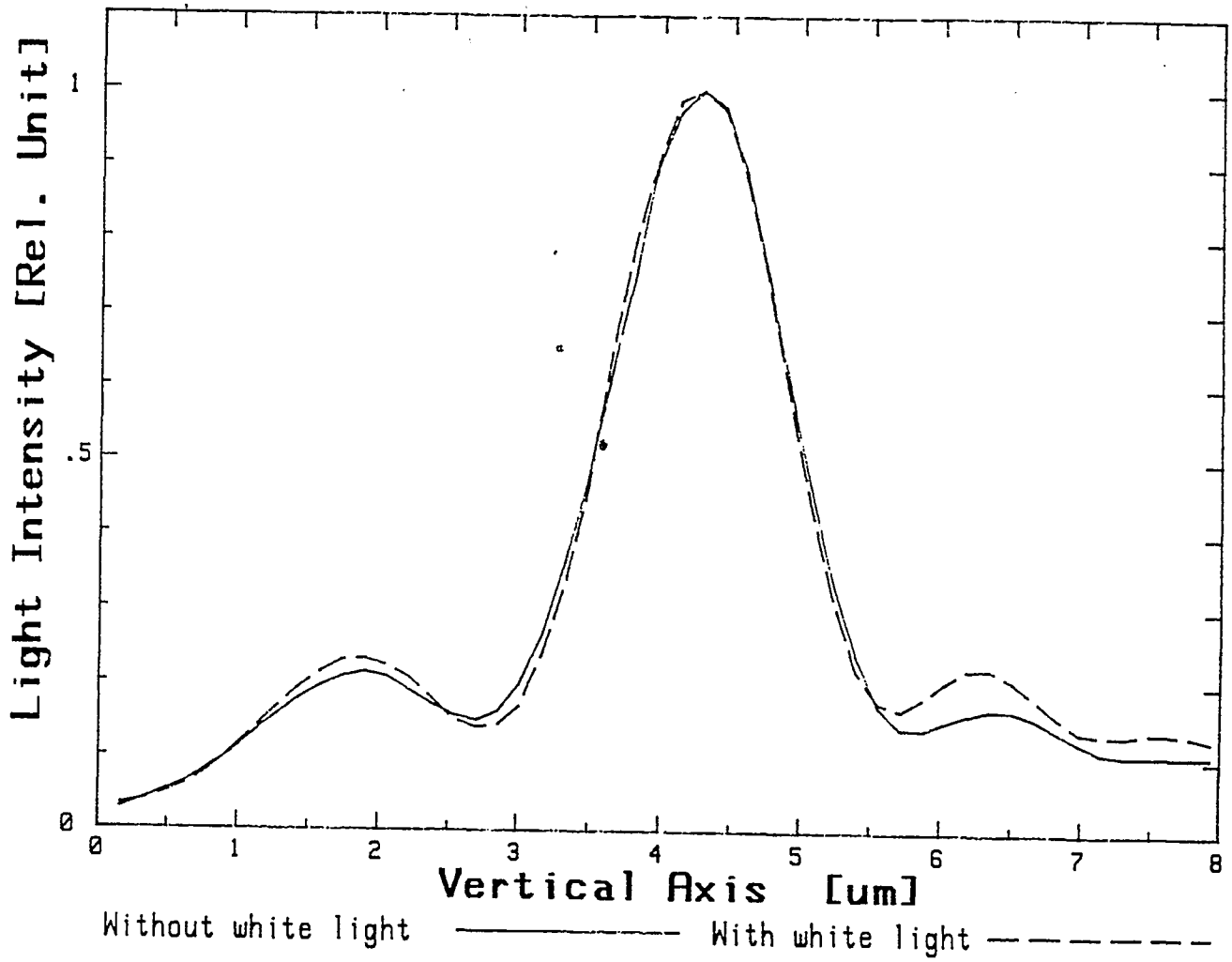

Fig.5-13. The near-field pattern of PMMA-CdS-PMMA waveguide in TM mode. The deposition time is 2 mins.

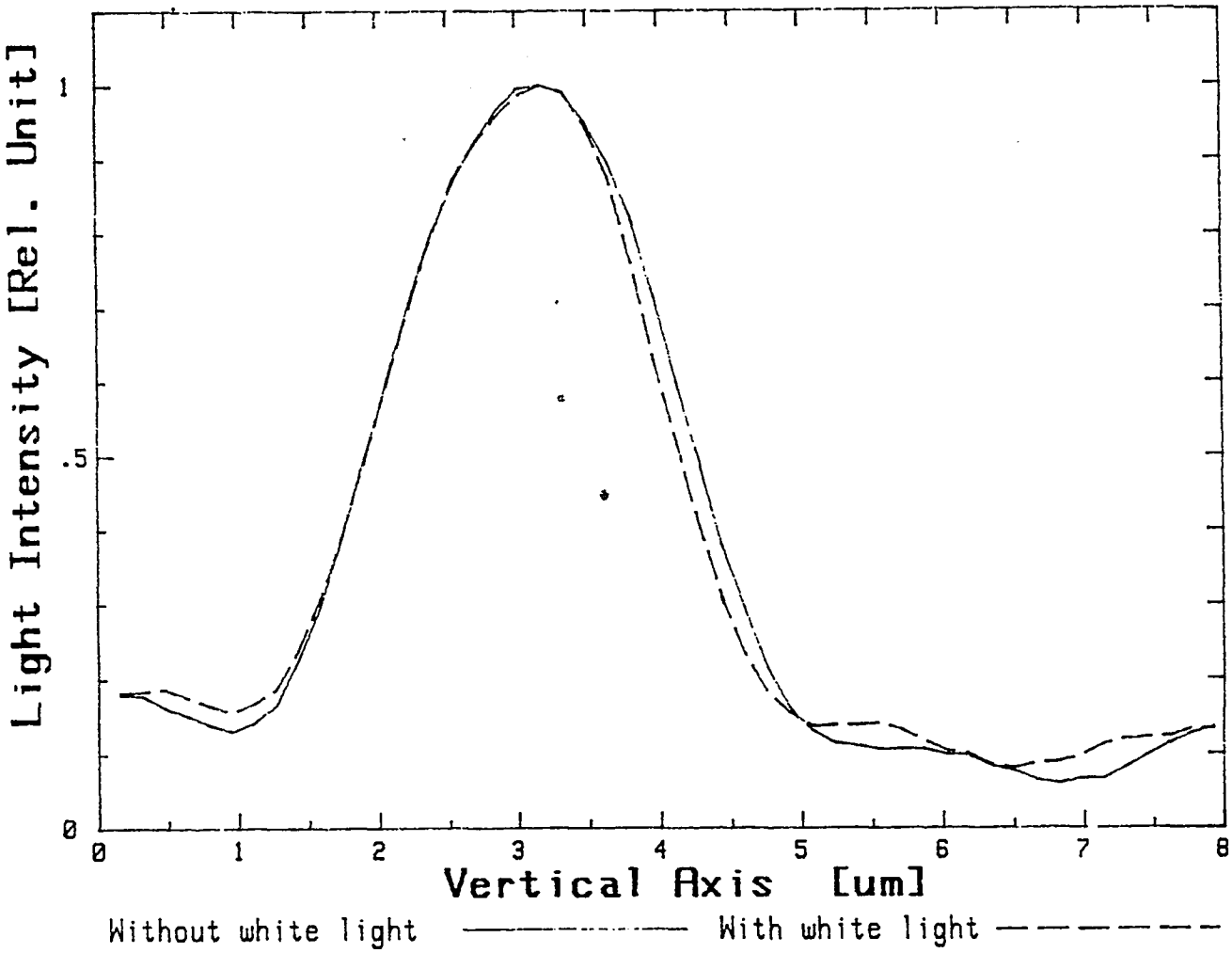

Fig.5-14. The near-field pattern of PMMA-CdS-PMMA waveguide in TM mode

The deposition time is 3 mins.

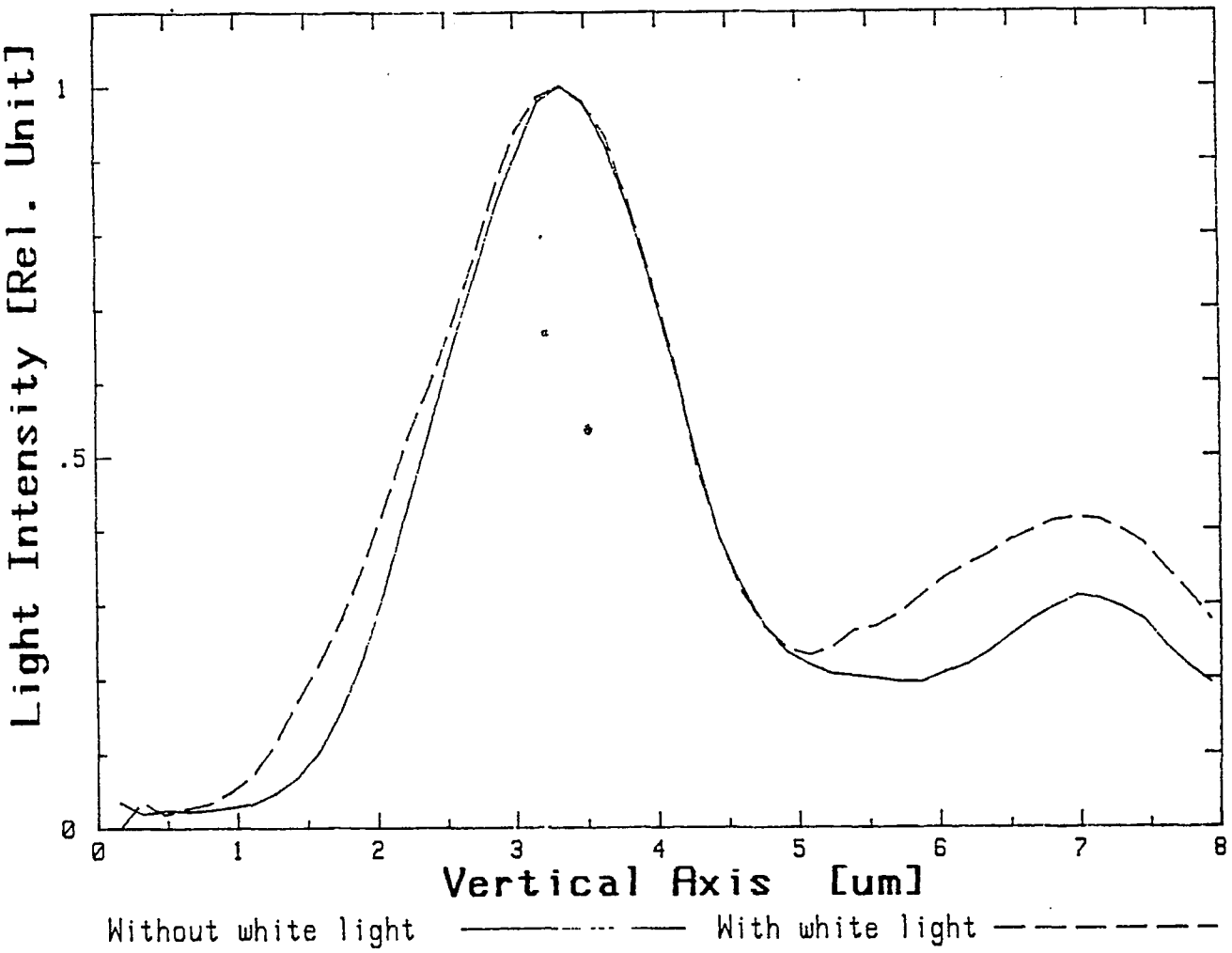

Fig.5-15. The near-field pattern of PMMA-CdS-PMMA waveguide in TM mode

The deposition time is 4 mins.

5.4.3 Control Experiment

The purpose of this experiment was to verify that the change of the near-field pattern of the waveguide was due to the presence of the CdS clusters. We prepared two samples under the same conditions. One was deposited with a CdS film, while the other was heated by an empty crucible. The results are shown in **Fig.5.16** and **Fig.5.17**. After normalizing the peak intensities with and without white light illumination no significant difference in the waists of the pure PMMA waveguide is seen. Later, we realized that a proper red filter (λ = 0.63 μm) may be used to eliminate the scattered light noise. Indeed, the results of cycle measurement show that this filter eliminated the need for profile normalization which in turn justified our normalization approach.

5.4.4 Cycle Measurement

During the experiment, we found an interesting effect: beside the waist and intensity differences with white light and without white light illumination , the near-field pattern of the waveguide shifted after light illumination. We made a cycle measurement to observe the shift of the near-field pattern of the waveguide after light illumination. In the cycle measurement, we measured the near-field pattern of the waveguide before white light illumination, with white light illumination, immediately after the light was turned off, and after the light was turned off for 10 minutes. In these measurement,

we put a filter in front of the detector to reduce the background noise. The filter transmitted only the light wavelength of 0.63 μm near the He-Ne laser wavelength. The results are shown in Fig. 5-18. Also, we increased the distance between the white light source and the waveguide sample from 1 cm to 9.5 cm in order to reduce the heat effect of the white lamp. The results are shown in Fig.5-19. We found that the near-field pattern of the waveguide shifted to the left side after white light source was turned off, but after certain time it shifted back to the right side of the original position of the waveguide near-field pattern.

In order to understand whether the shift of the near-field pattern of the waveguide was due to white light illumination or heat effect, we illuminated the waveguide sample for a very short time (3 ~ 5 seconds). With such short time the white light source would not have enough time to heat the waveguide sample.The result is shown in Fig.5-20 and we still can observe the near-field pattern of the waveguide shift to the left side.

5.4.5 Stroboscope as a Pump Light

In this measurement, the procedure of measurement was the same as before, but we used a stroboscope to substitute the incandescent white light source. Two stroboscope frequencies were used in this experiment, one was 130 ppm and the other was 13000 ppm (pulse per minutes). Here, we used the same waveguide (PMMA-Cds-PMMA) and the

results are shown in **Fig.**5-21, **Fig.**5-22,and **Fig.**5-23. The near-pattern of the waveguide in TM mode shifted to left side after the light was turned off in both frequencies. We did not see any change in TE mode in this measurement. **Fig.**5-24 showed the pure PMMA waveguide pattern did not change in this experiment.

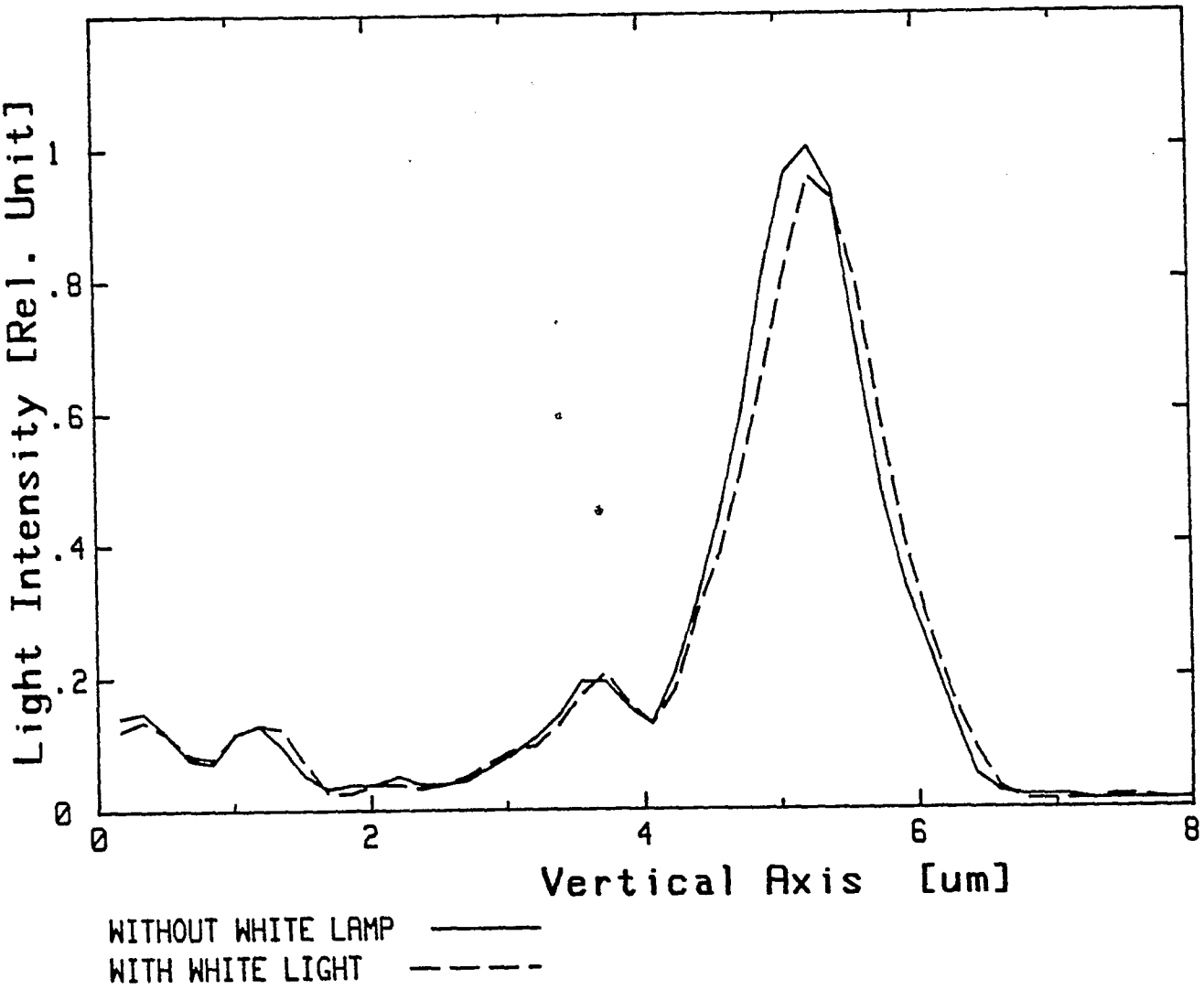

Fig.5-16. The near-field pattern of pure PMMA-PMMA waveguide in TE mode.

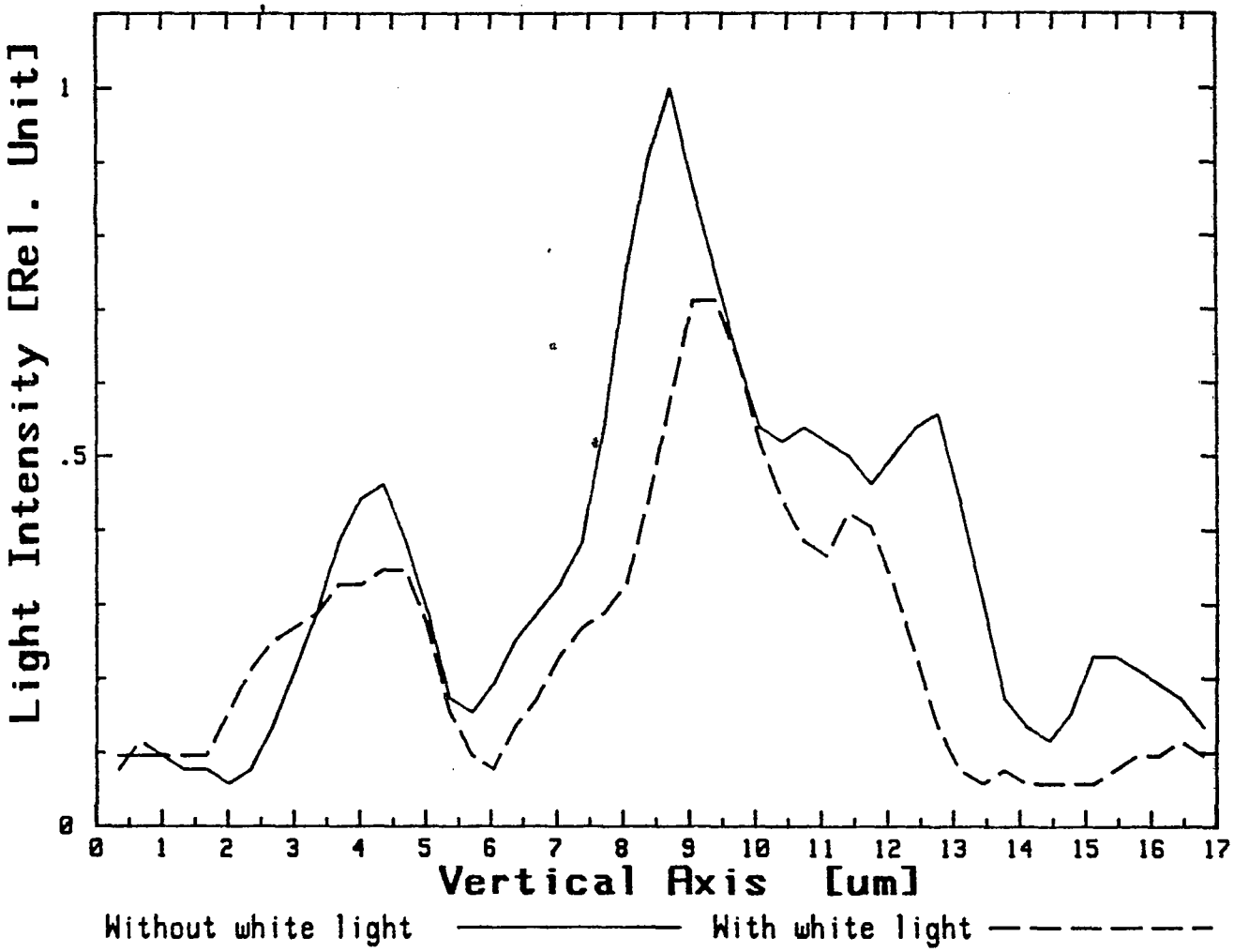

Fig.5-17.The near-field pattern of PMMA-CdS-PMMA waveguide.Shown is the TE mode.

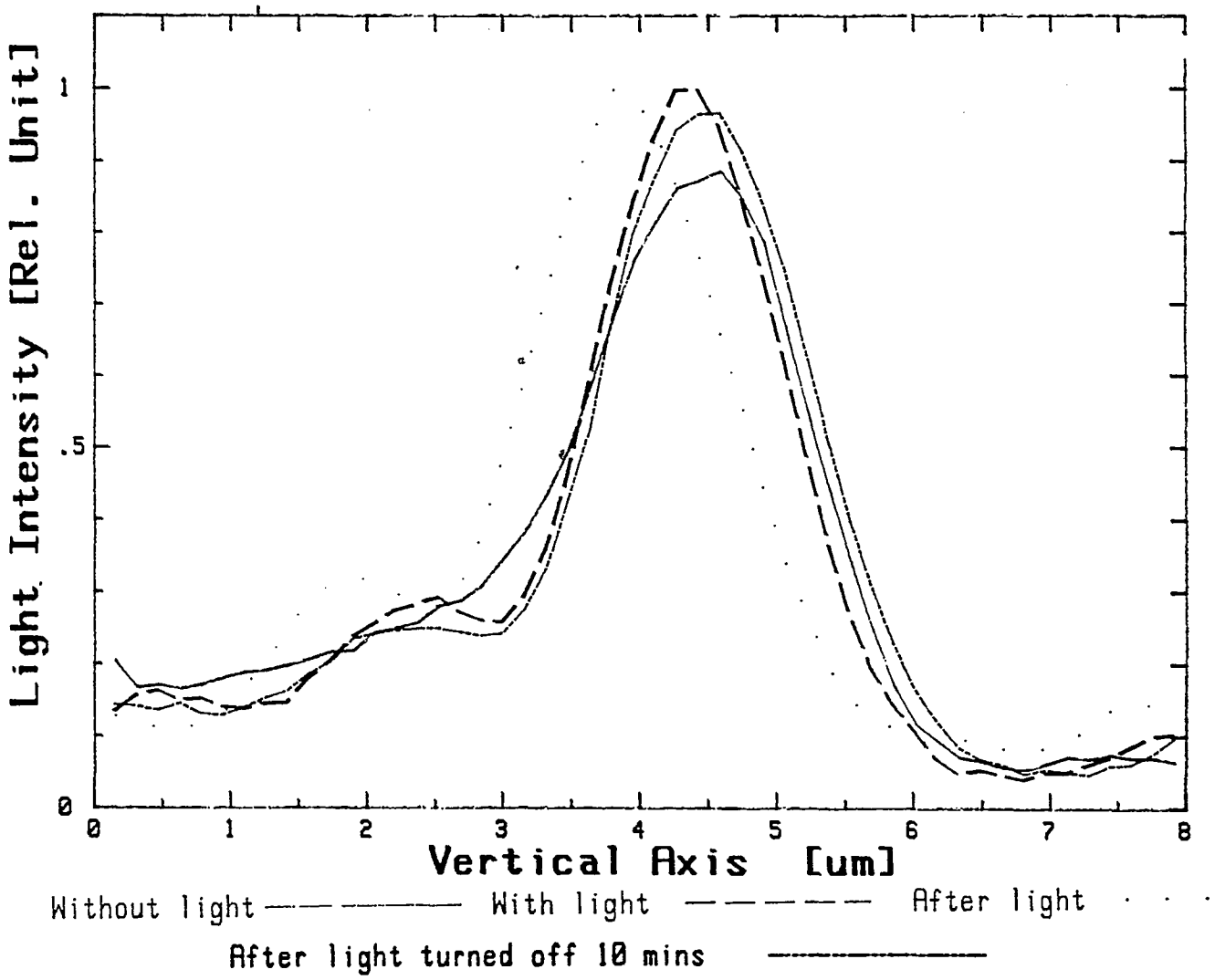

Fig.5-18. The results of cycle measurement of a TE mode

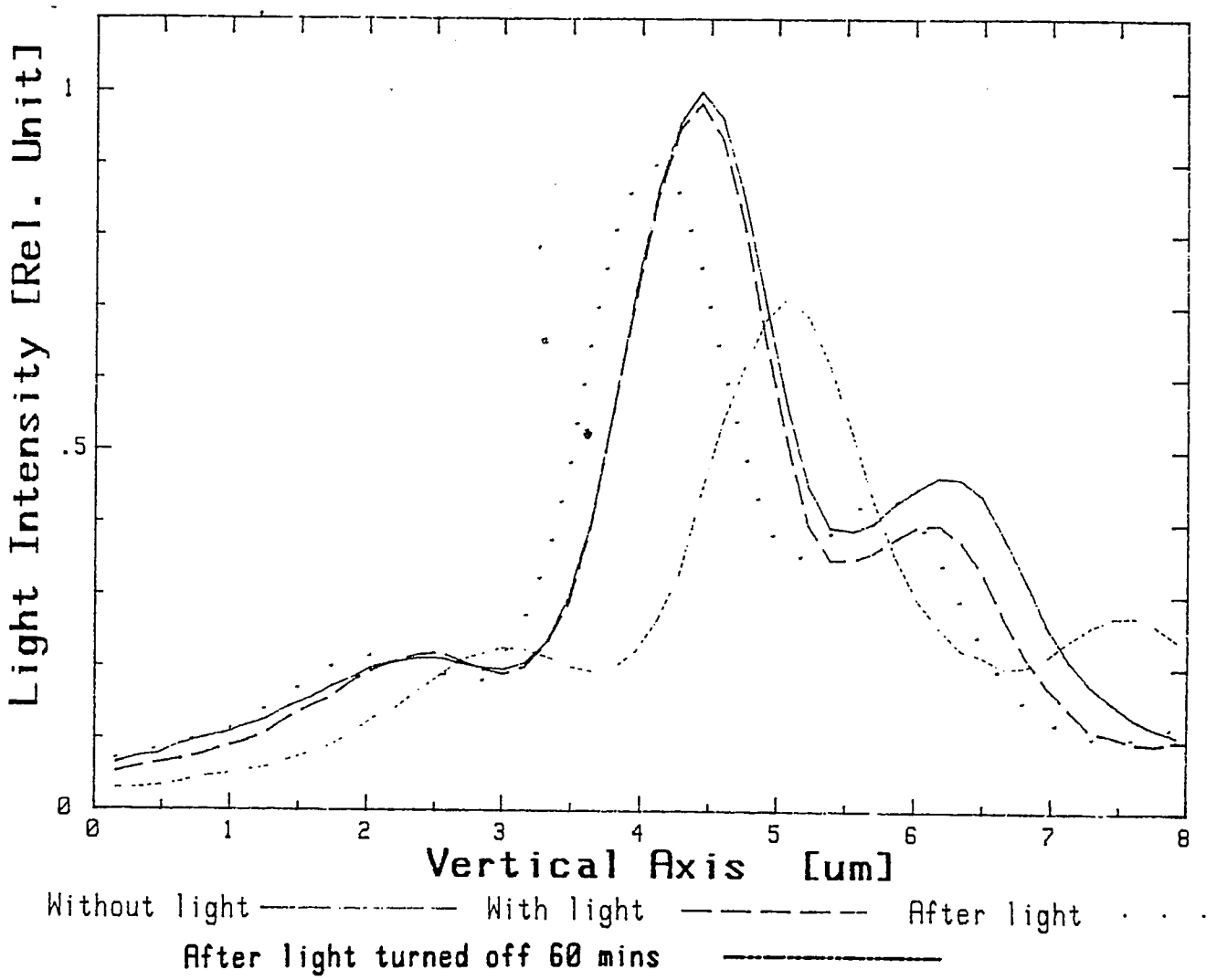

Fig.5-19. The results of cycle measurement where the distance between light source to the sample is increased.

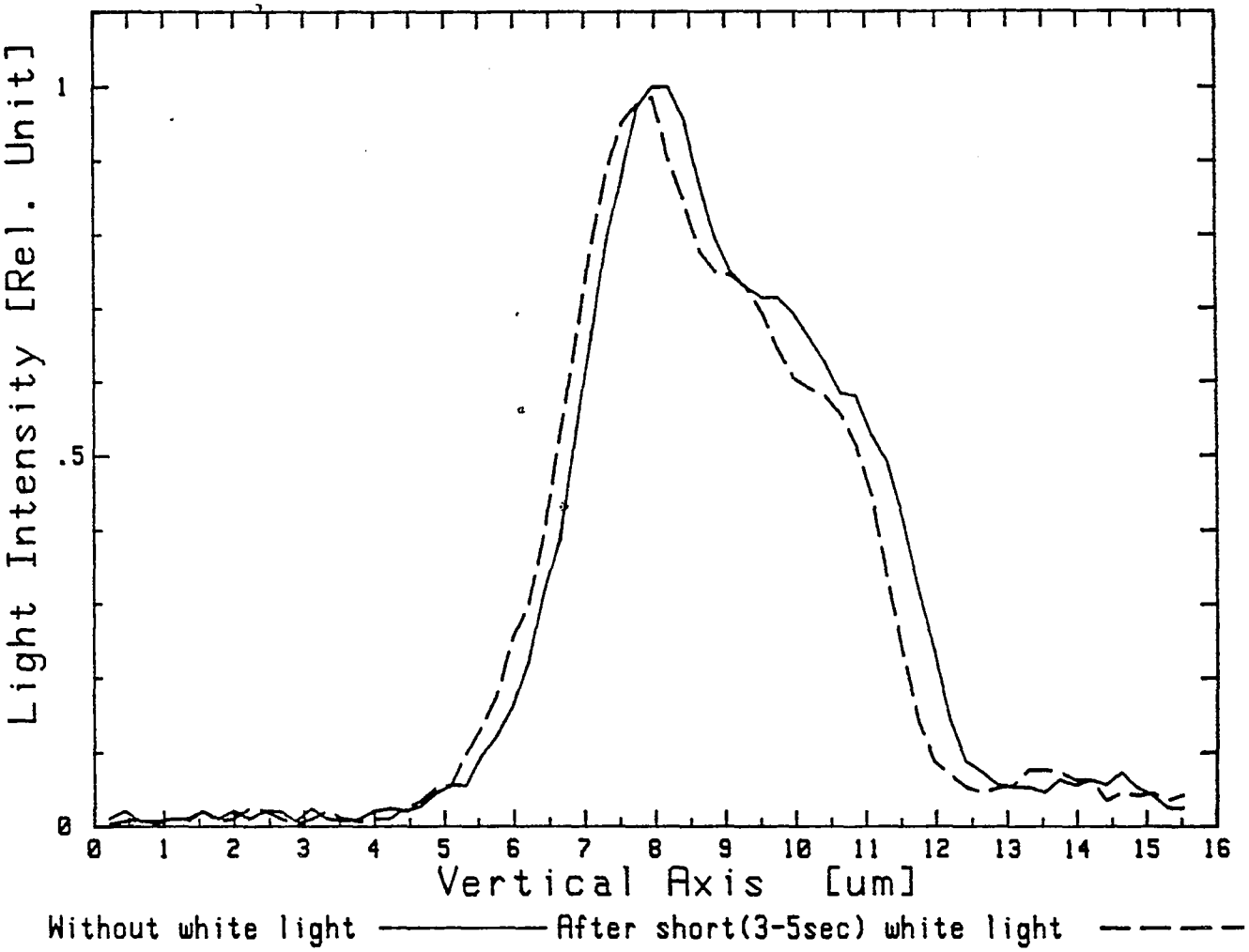

Fig.5-20. The near-field pattern of the waveguide after short white light illumination time(3 ~ 5 sec).

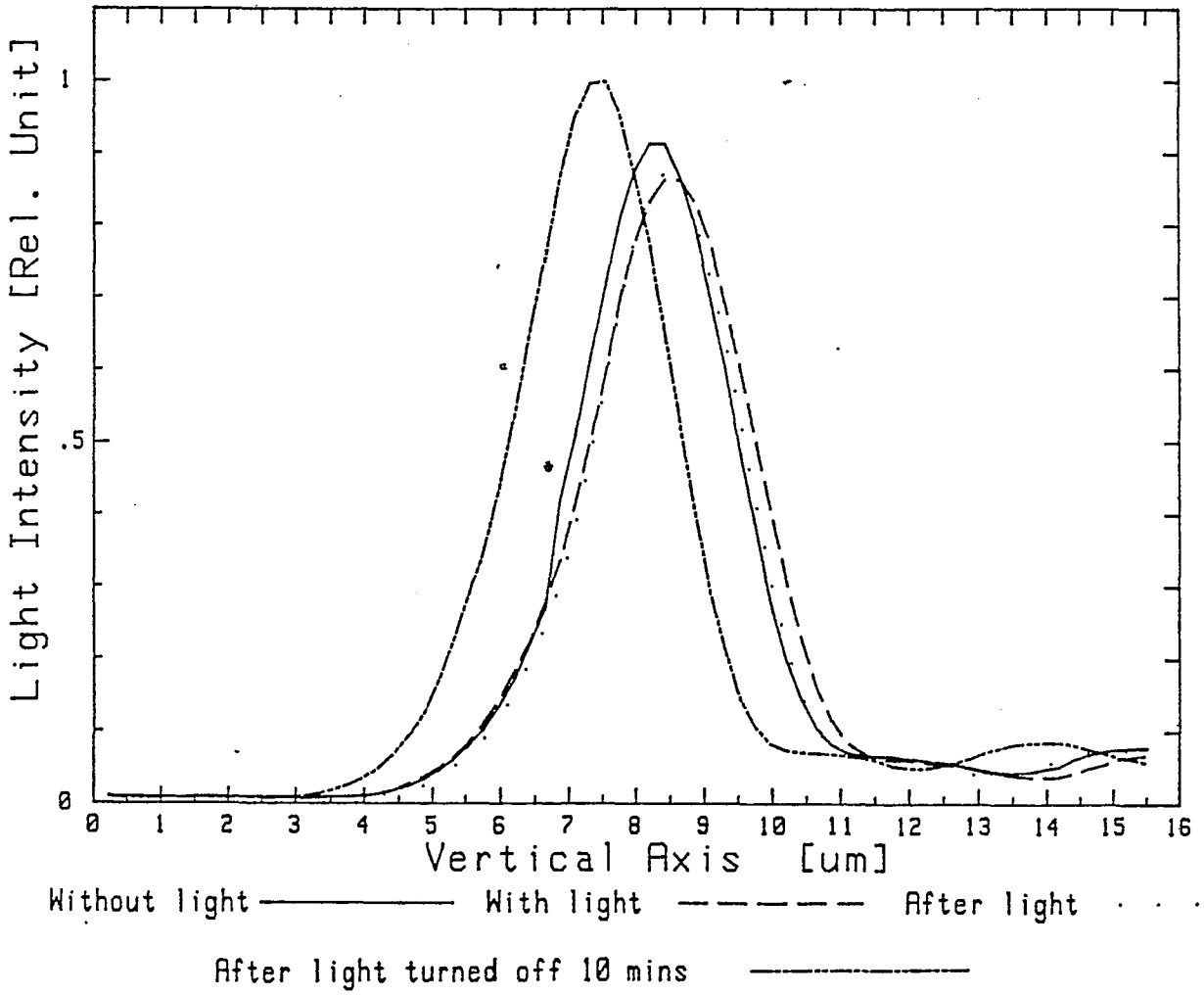

Fig.5-21. The near-pattern of a TM mode in a PMMA-CdS-PMMA waveguide. The frequency of stroboscope is 130 ppm (pulse per minutes).

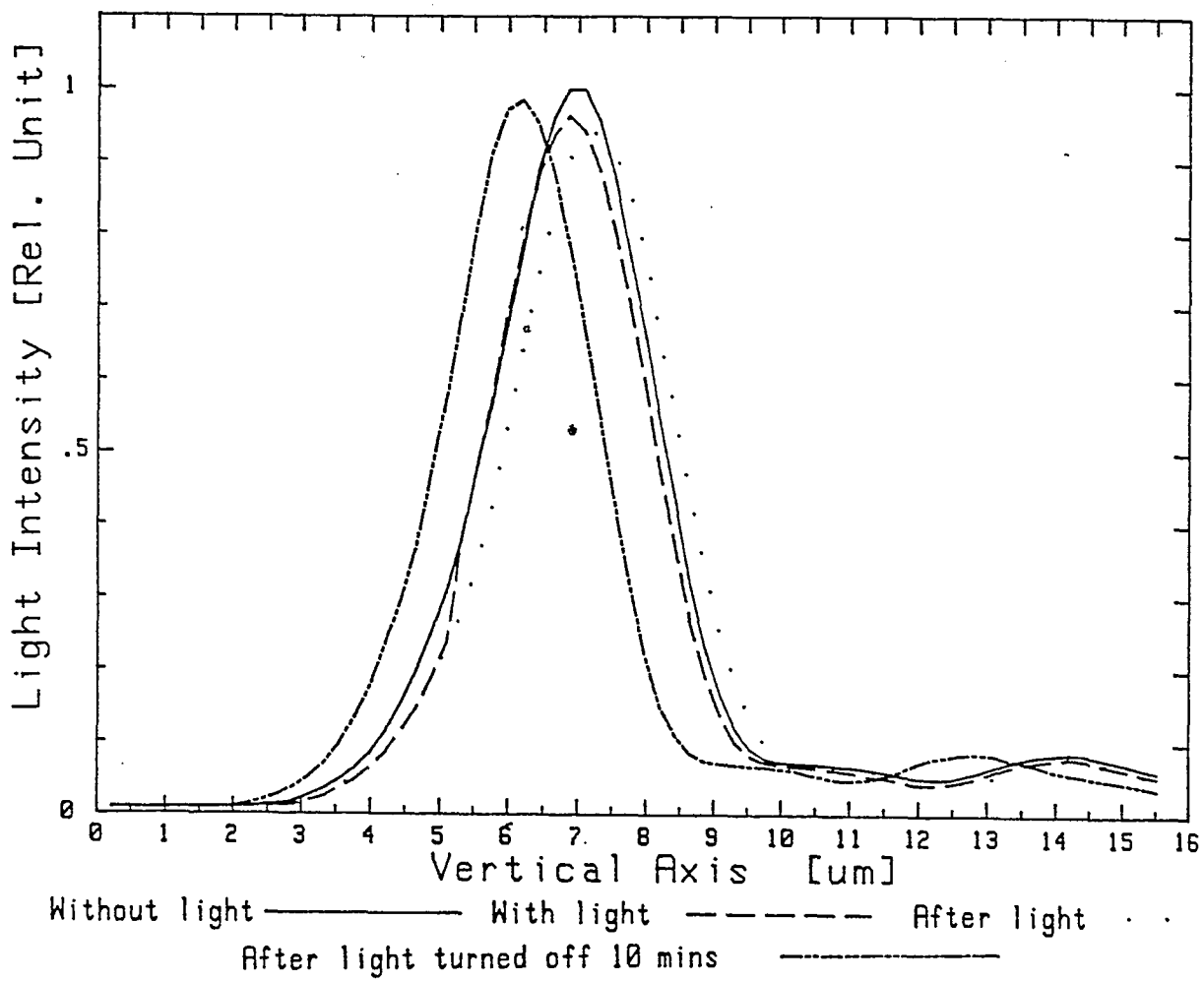

Fig.5-22. The near-pattern of a TM mode in a PMMA-CdS-PMMA waveguide. The frequency of stroboscope is 13000 ppm.

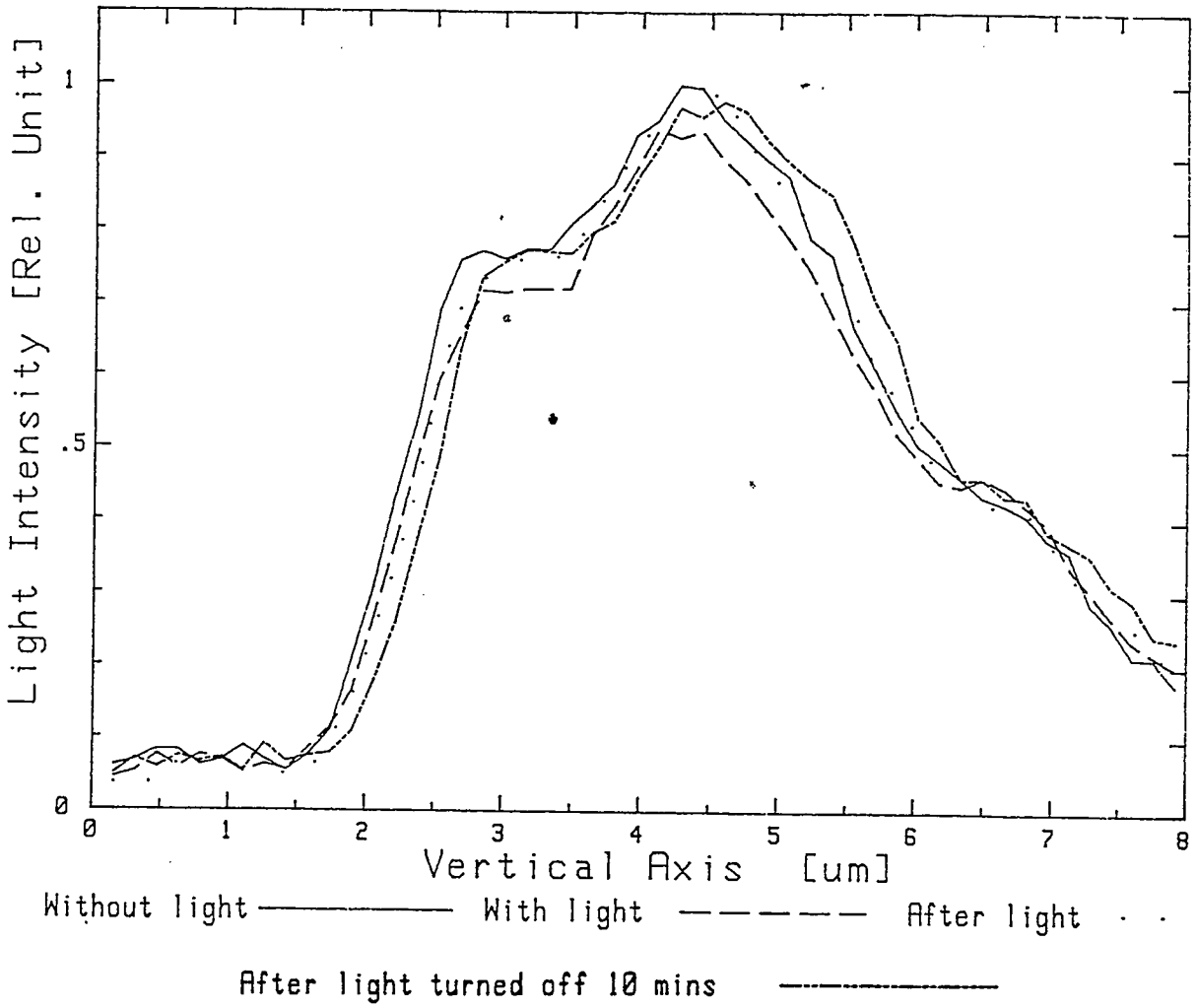

Fig. 5-23. The near-pattern of a TE mode in a PMMA-CdS-PMMA waveguide. The frequency of stroboscope is 13000 ppm.

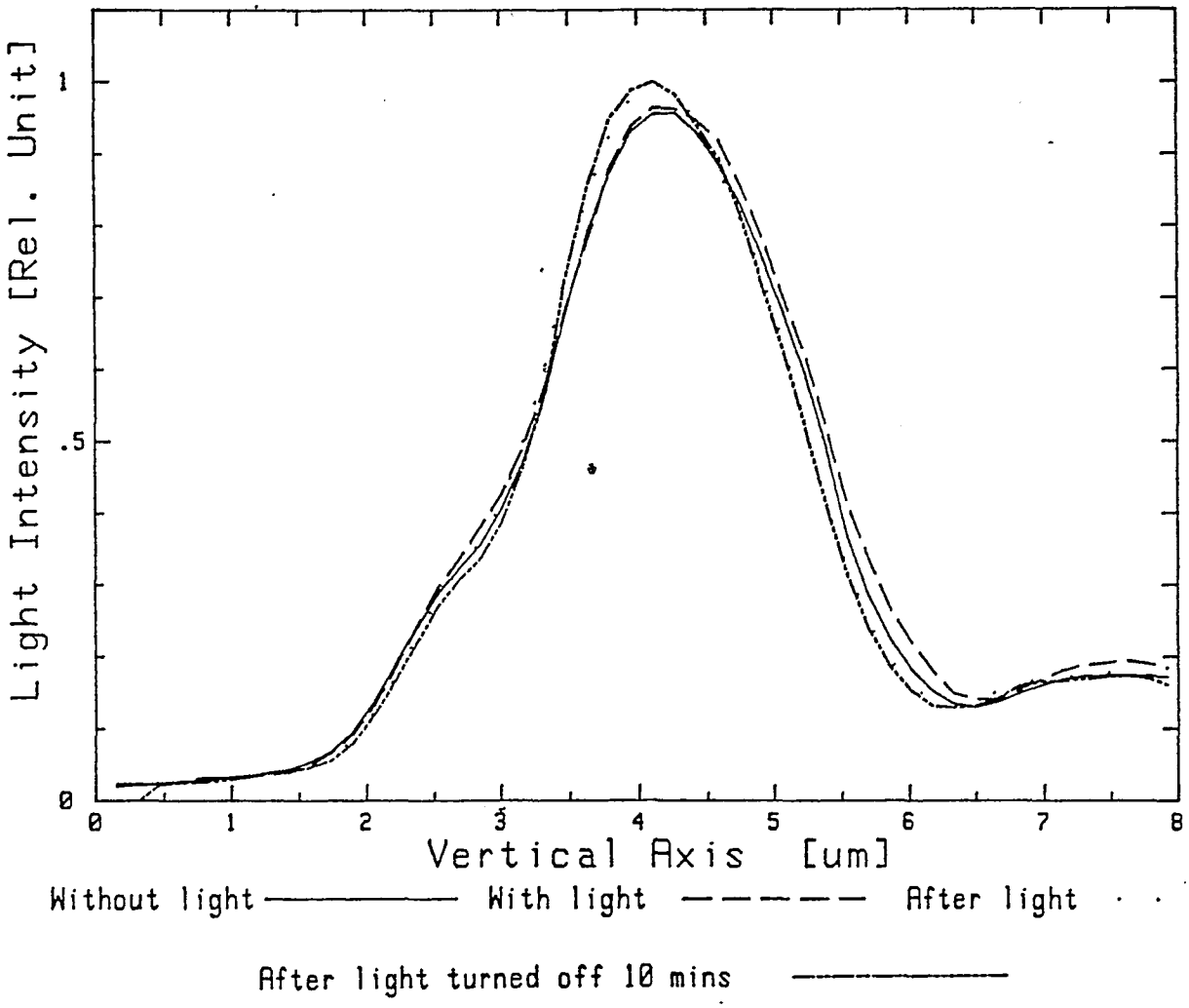

Fig.5-24. The near-pattern of a TM mode in a pure PMMA waveguide.

The frequency of stroboscope is 130 ppm.

Chapter 6 Discussion

6.1 Film Deposition

6.1.1 Plasma Deposition

We investigated the relationship between deposition time, pressure, and film thickness in a discharge chamber. The results showed that the plasma deposition is halted after 60~70 minutes. This effect might be caused by the increased temperature of the film surface. As the temperature is increased, the etching process starts to take place. This may be a problem when continuously growing a film of more than 3 μm thick. Fig.5-1 shows that the maximum film thickness was about 2.2 μm after 60 minutes of plasma deposition. In order to overcome this problem , we stopped the deposition process after 60 minutes, let the substrate cool down and continue the deposition. In this way, we could achieve film thickness of 4 to 6 μm.

Film thickness is proportional to the pressure inside the chamber and the pressure is proportional to the flow rate of the monomer. At higher pressures, there are more monomer molecules available for plasma polymerization and this results in a higher deposition rate as

shown in Fig.5-2.

6.1.2 Vapor Deposition

We observed CdS clusters on a PMMA film surface using Scanning Electron Microscope. In order to achieve the novel dielectric properties, the cluster size of an artificial dielectric material should be smaller than the optical wavelength used. In our case it is much smaller than 0.6328 μm, the laser spectral line.

The results of RBS measurement of the sample deposited for 3.5 minutes (sample B) give an average CdS film thickness of 435 Å. The sharp CdS peak in the RBS spectrum indicates that the film thickness is uniform .(Fig.5-5)

RBS measurements of a sample deposited for 2 minutes (sample A) show that CdS material did not form a continuous film. This indicates that the critical thickness of forming a continuous film is above 248 Å calculated from the thickness of sample B and the deposition time ratio. It is possible that the sample made by 2 minutes deposition had less CdS material than calculated.

By interpretation the RBS measurement on sample B, we estimate the average film thickness of a sample deposited for 3 minutes as 370 Å. The clusters in the SEM images have equivalent thickness about 20 Å calculated by estimating the average cluster volume and the cluster

density. From these two results we conclude that some of the CdS are in cluster form and some of them are in a form of a continuous film. The cluster do not contribute significantly to the average film thickness.

6.2 Optical Measurement

(1) Changes in the waist intensity profile of PMMA-CdS-PMMA waveguide : From chapter 2, we know that the effective permittivity is a function of light intensity and the index of refraction is defined as:

$$n = \left(\frac{\varepsilon_{eff}\mu_{eff}}{\varepsilon_o \mu_o}\right)^{1/2}$$

μ_{eff} is the effective permeability. When ε_{eff} increases with increasing light intensity the index of refraction will increase too. Once we change the index of refraction n, we change the propagation properties for the probe optical beam (the He-Ne laser beam). We expect that the waist of near-field pattern of the waveguide will be narrowed with light illumination due to the effective increase in the refractive index of the CdS cluster.

From the measurement of the near-field pattern in Chapter 5, we indeed found that for a PMMA-CdS-PMMA waveguide under illumination by a white light source, its waist of the near-field pattern became narrower than without white light illumination. This may indicate that

the illumination by white light source changed the effective index of refraction of the waveguide. The lower the intensity of the white light illumination, the less this effect is.

In Fig.5-10 ~ Fig.5-15, we normalized the near-field pattern of PMMA-CdS-PMMA waveguide, under and under no white light illumination to unity, in order to eliminate the effect of the scattered light noise. The results of additional test measurements supported the normalization approach. When a red filter to eliminate the scattered light noise was used, the peaks of the near-field pattern of PMMA-CdS-PMMA waveguide under and under no white light illumination were almost the same.

To examine whether the change in the properties of the waveguide were due to the presence of the CdS and not an artifact of the film processing, we performed a control experiment to compare two waveguides. One had two layers of PMMA and the other had a thin layer of CdS film between two layers of PMMA. The results of the near-field intensity pattern shown in Fig.5-15 and Fig.5-16 indicate that the waist of the near-field pattern of a pure PMMA waveguide was not affected by the white light source illumination. Both the intensity and the waist of the near-field pattern of PMMA-CdS-PMMA waveguides were affected by the white light. Thus we conclude that the profile waist narrowing is indeed due not to the optical loss, but to the interaction of the white light illumination with the CdS layer, which caused the dielectric constant change.

(2) The effect of the cluster size : We used TEM, SEM and RBS to measure the film thickness. In TEM measurement, we failed to make a specimen of CdS on PMMA which is less than 1000 Å in total thickness necessary for the TEM measurement.

From SEM and RBS measurements, we may estimate the distribution of CdS for different deposition time. Table.6-1 lists the waveguide optical profile waist change with different deposition time in TE mode and different distributions of CdS film.

Table.6-1 The waveguide waist change in TE mode and different distributions of CdS film

waveguide waist change(μm)	the distribution of CdS
0.296	discontinuous film, islands
0.135	a very thin film between clusters
0.082	continuoes film

The biggest waveguide waist change occurred when a discontinuous CdS film embedded into two layers PMMA. Almost no change occurred in waveguide waist when a continuous CdS film embedded into two layers of PMMA. H.Grebel[10] suggested that skin-depth effects put an upper limit on the cluster size of approximately 0.01λ. At these sizes the characteristics of the artificial dielectric waveguide at optical frequencies will therefore be determined by the conductivity properties of the guest material as well as the optical properties of the host waveguide material.

(3) Shift effect: In the cycle measurement, we found that the near-field pattern of the waveguide slowly drifted a long time. These results are shown in **Fig.**5-18 and **Fig.**5-19. Thermal effects have been eliminated by increasing the distance between the white light source and the sample. Figure 5-19 shows that , nevertheless, the profile shift still exist even for low white light intensity illumination. The shift effect also exist when we used a short time light pulse (3 ~ 5 sec) to illuminate the sample.

Using a stroboscope as a pump light showed that the intensity profile of the waveguide for TM mode was shifted after the light was turned off at two light pulse frequencies and with no substantial change in the TE mode. The waveguide waist did not change for both PMMA- CdS - PMMA and pure PMMA waveguide. The light intensity of the stroboscope was about 0.2 w which was smaller than that of the 150 w white light source (10 w of light power).

A possible explanation to the above phenomena of profile shift is charge migration. Carriers are generated by the pump light. As the pump light is turned off, the charge migrate to all directions. For unknown reasons, the center of this migration process oscillates as shown in **Fig.**5-19.

Chapter 7 Conclusion and Future Work

We have demonstrated that the properties of a waveguide consisting of a thin layer of CdS embedded into a PMMA were changed by the illumination of a white (pump) light source. The waist of the near-field intensity pattern of the waveguide was changed up to 15% in a clustered CdS film under the illumination from a white light source. The results show that the waveguide waist change is not proportional to the quantity of the CdS but may have an optimal value as a function of the cluster size.

For future works, we suggest to extend the guest material to other II-VI semiconductor materials and to other host materials such as glass or quartz.

REFERENCES

1. M.S. Htoo, *Microelectronic Polymers,* Marcel Dekker, Inc.(1987)
2. D.B.Ostrowsky, and A.Jaques, *Formation of Optical Waveguiges in Photoresist Films, Appl.Phys.Lett.* **18**,556. (1971)
3. R.Ulrich, and H.Weber, *Solution-Deposited Thin Films as Passive and Active Light-Guides, Appl.Opt.* **11**,428. (1972)
4. T.Sosnowski,and H.Weber, *Thin Birefringent Polymer Films for Integrated Optics, Appl.Phys.Lett.* **21**,310. (1972)
5. D.A.Ramey,and J.T.Boyd, *Polyurethane Fan-Out Channel Waveguide Array for High Resolution Optical Waveguide Imaging, IEEE.Trans.CAS*-26,1041 (1979)
6. D.L.Lee, *Electromagnetic Principles of Integrated Optics,* John Wiley & Sons,New York,1986,p174.
7. P.K.Tien, G.Smolinsky,and R.Martin,*Thin Organosilicon Films for Integrated Optics, Appl.Opt.* **11**,673. (1972)
8. A.Yariv,P.Yeh, *Optical Waves in Crystals* ,John Wiley & Sons,New York,1984 ,p.416-419.
9. R.E.Collin,*Field Theory of Guide Wave,*McGrawhill,New York,1960. p512-515.
10. H.Grebel and P.Chen, *Artifitial Dielectric Polymeric Waveguides : Semiconductor- Embedded Films,*Opt. Lett.15,667-669.(1990)
11. H.Yasuda,*Plasma Polymerization,*Academic Press,New York,1985.
12. H.Yasuda and T.Hiyotsu, *Distribution of Polymer Deposition in Plasma Polymerization. II. Effect of Reactor Design, J. Polymer*

Sci. Polymer Chem. Ed., 16 , 313 . (1978)

13. H. Yasuda and T. Hirotus, *Distribution of Polymer Deposition in Plasma Polymerization. I. Acstylene, Ethylene, and the Effect of Carrier Gas, J. Polymer Sci. PolymerChem. Ed,* 16 , 229 . (1978)

14. H. Yasuda and C. E. Lamaze, *Polymerization in an Electrodeless Glow discharge. II. Olefinic Monomers, J. Appl. Polymer Sci.,* 17 , 1519. (1973)

15. L. F. Thomson and K. G. Mayhan, *The Plasma Polymerization of Vinyl Monomers. II. A Detailed Study of t he Plasma Polymerization of Styrene, J. Appl. Polymer Sci.,* 16, 2317. (1972)

16. H. Yahuda and C. E. Lamaze, *Polymerization of Styrene in an Electrodeless Glow Discharge. J. Appl. Polymer Sci.,* 15, 2277. (1971)

17. R. F. Bunshah and C. V. Deshpandey, *Evaporation Processes, Mrs Bulletin,* Dec. 1988.

18. L. I. Maissel, R. Glang(ed.) , *Handbook of Thin Film Technology* , McGraw-Hill, 1983, p. 8-32 ~ 8-36.